Studies of SiPM properties using an integrating sphere

von

Jan-Frederik Schulte

Bachelorarbeit in Physik

vorgelegt der
Fakultät für Mathematik, Informatik und Naturwissenschaften der RWTH Aachen
im März 2010

angefertigt am
III. Physikalischen Institut A der RWTH Aachen
Prof. Dr. Thomas Hebbeker

Zusammenfassung

Der Siliziumphotomultiplier (SiPM) ist ein relativ neues Gerät zum Nachweis von Photonen bei sehr niedriegen Photonraten. Er hat gewisse Vorteile im Vergleich zu traditionellen Photomultiplierröhren (photomultiplier tubes, PMTs). Da er auf Halbleitertechnologie basiert, schätzt man den SiPM für seine geringe Größe, Unempfindlichkeit gegenüber Magnetfeldern und seine relativ niedrigen Kosten verglichen mit PMTs. Dies eröffnet ihm ein weites Feld von Anwendungen in der Teilchenphysik, zum Beispiel in zukünftigen Upgrades der Detektoren des LHC. Für die Entwicklung von Prototypen in dieser Richtung müssen die Eigenschaften des SiPM gründlich verstanden werden. Diese Arbeit beschreibt die Entwicklung eines Versuchsaufbaus in dem eine Ulbrichtkugel den SiPM und einen Referenzdetektor mit diffusem Licht versorgt um zu versuchen Eingeschaften des SiPM, wie etwa die Photonnachweiseffizienz (photon detection efficiency, PDE), zu studieren.

Abstract

The Silicon Photomultiplier (SiPM) is a relatively new device for photon detection at very low photon rates. They have certain advantages compared to the traditional photomultiplier tubes (PMT). As they are based on semiconductor technology, SiPMs are appreciated for their small size, indifference to magnetic fields and their relatively low costs compared to PMTs. This opens a wide field for the application of the SiPM in particle physics, for example in future upgrades of the LHC detectors. For the development of prototypes in this direction, the properties of SiPMs have to be profoundly understood. This thesis describes the development of a test stand in which an integrating sphere is used to provide the SiPM and a reference detector with the same amount of diffused light to try to study properties such as the photon detection efficiency (PDE).

Contents

1. Introduction

Driven by the goal to fully understand its enviroment, mankind has come a far way from the first observations of nature in ancient Greece. After the great successes of science, especially physics, following the development of its fundamental principles in the 17th and 18th century, scientists were forced to leave the areas where they were able to test their theories by observation of what was directly visible to them. To make any statements about the phenomena of interests, more and more complex and sophisticated measurement instruments had to be developed. When physicists began to investigate the world on an atomic and subatomic level, the ability of detecting single photons became a necessity. In the 1930s this became possible by the development of Photomultipliertubes (PMTs). They use the photo effect to generate a single electron when the photon hits the photocathode of the tube. This electron is then multiplied by hitting several dynodes on its way to the anode. A gain of up to 100 million is possible.
This technique has several limitations which make it necessary to develop alternative detectors. The most severe drawbacks of a PMT are the need to use high voltage up to 2000 V, the rather great size of the tube, the high price due to the high amount of precision work needed in the production and the sensitivity to magnetic fields.

In recent years a new detector has entered the world of experimental physics that solves this problems and thus has become a much appreciated tool in many laboratories. It is named silicon photomultiplier (SiPM) and uses one of the most prominent features of semiconductors, the p-n junction. SiPMs can be used in most experimental setups where the use of conventional PMTs is not possible for some reason.

As this new detector technology is highly popular, many researchers have started to work with them and to develop first applications. To use them it is necessary to fully understand their properties under various conditions, which requires a thorough testing of many parameters. Goal of this thesis is to develop a test stand with which it will be possible to measure the response of an SiPM to the light of an ultraviolet LED. One of the parameters that will be investigated is the photon detection efficiency (PDE), which is the probability of the SiPM to detect an incident photon. To determine this value, information on how many photons were detected by the SiPM and how many actually reached it. To obtain a value for the latter, a calibrated PIN diode is used as a reference detector. To ensure that both detectors are exposed to the same amount of photons an integrating sphere is used to diffuse the light of the LED.

This thesis will described the physical principles on which the detectors are based and the properties of the experimental setup. This is followed by an examation of basic properties of the hardware used in the test stand an the first results obtained from measurements with the full setup ready.

2. Theoretical Foundations

The SiPM is able to measure the photon flux on single photon level, thus being far more sensitive than conventional photodiodes. Both are based on the same physical principles utilizing the unique properties of the p-n junction in semiconductors. This chapter will describe the underlying physical concepts and the development of photon detectors based on them.

2.1. The Semiconductor

In single atoms, each electron occupies a discrete energy level. If N atoms of an element form a crystal lattice, these energy levels are N times degenerate [Lutz]. As it is forbidden for fermions to occupy the same quantum mechanical state by the Pauli principle, the energy levels split. As the number of atoms in a solid is very large, the many only slightly different energy levels form energy bands, in which it is allowed for electrons to occupy states. These bands can be divided by forbidden zones, the band gaps. The size of the band gap E_g usually refers to the minimal difference of energy between the two bands

Electrons fill the possible energy levels according to the Fermi distribution, with E_F being the Fermi level [Lutz]:

$$f(E) = \frac{1}{e^{\frac{E-E_F}{kT}} + 1}. \tag{2.1}$$

Figure 2.1 shows this process for the example of silicon. The different energy levels split to form

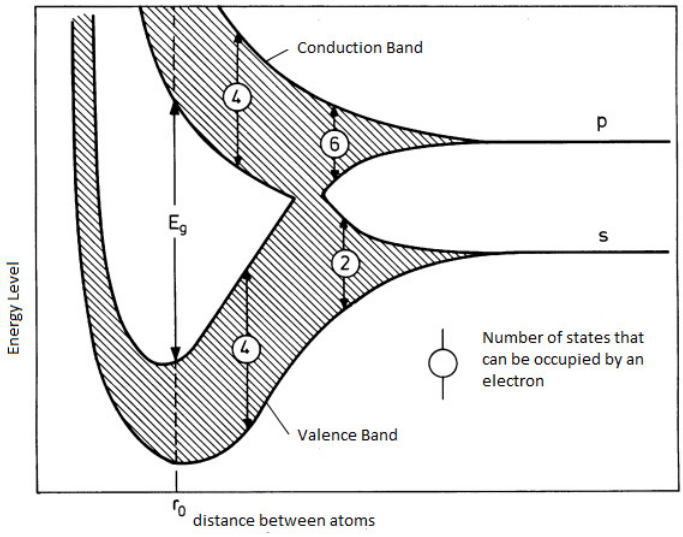

Figure 2.1.: *Forming of energy bands in Silicon [Ibach09]*

bands as the atoms get closer together.
Important for the conductivity are the valence band and the conduction band. The valence band is the highest energy band occupied by electrons at a temperature of zero Kelvin. The conduction band lies above it. Electrons in this band contribute to the conductivity, because they are not bound to a specific atom in the lattice. In conductors the two bands overlap or the conduction

band is partly filled, so there are always many electrons in the conduction band. In insulators the band gap between them is larger than about 4 eV and the conduction band is unoccupied.
This difference in the band gap is illustrated in figure 2.2.

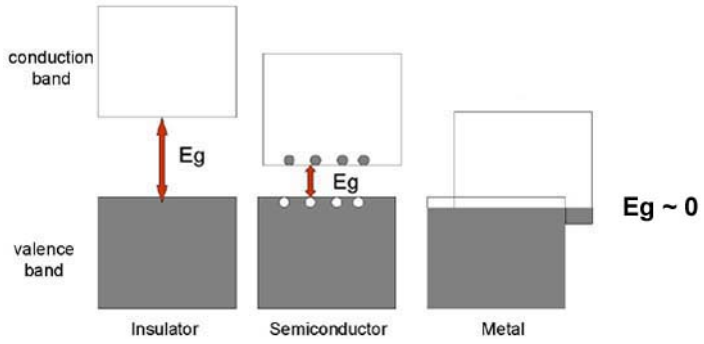

Figure 2.2.: *Metal, Semiconductor and Insulator classified by band gap [Wisc]*

Semiconductors have a relatively small band gap. Therefore it is possible to excite electrons, as seen in figure 2.3, into the conduction band where they contribute to the conductivity as a negative charge carrier. In the valence band they leave behind an unoccupied state, called hole, which is a positive charge carrier. It is in good approximation possible to treat holes and electrons as if they

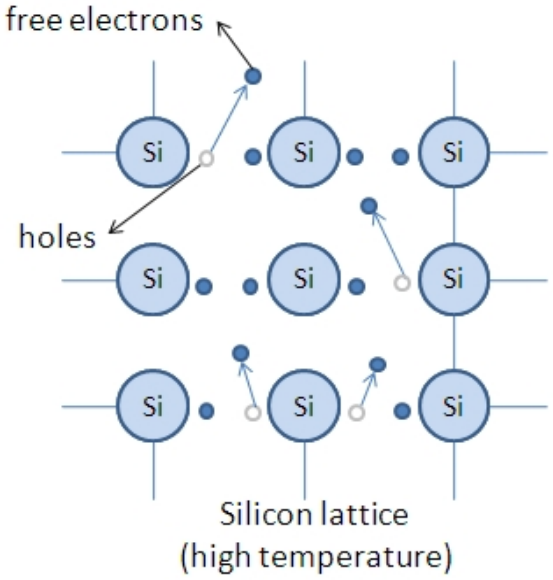

Figure 2.3.: *Excitation of electrons in silicon*

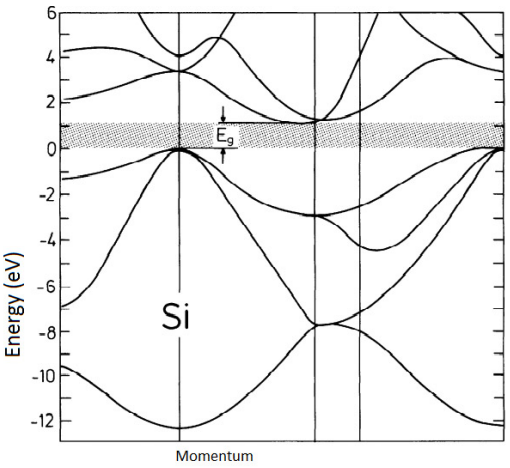

Figure 2.4.: *Schemactic of the band structure in silicon [Ibach09]*

were free charge carriers indifferent of the lattice structure of the semiconductor, if their free mass is replaced by an effective mass that incorporates all those effects.
A distinction has to be made between direct and indirect semiconductors. In the direct semiconductor, minimal size of the band gap is between states with the same momentum. An excitation with an energy higher than this size is enough to lift an electron into the conduction band. In an indirect semiconductor the minimal band gap is between states with different momentum. A additional momentum of a phonon or an energy high enough to cross the band gap at the given momentum is needed to lift an electron intro the conduction band. Silicon is an indirect semiconductor as can be seen in figure 2.4.

Silicon is widely used in all modern electronics and its properties are the basic of the silicon photomultiplier. Some semiconductor have very small band gaps, for example germanium with 0.67 eV at a temperature of 300 K, and thermal energy is sufficient to lift electrons into the valence band. Silicon however has a band gap of 1.12 eV at 300 K and thermal excitation of electrons is nearly impossible [Lutz].

One of the most important properties of semiconductors is the possibility to modify the structure of the band gap and thus the conductivity according to the requirements of the application. This is done by the so called doping, which means that impurities are added into the lattice structure of the semiconductor. For this purpose elements are used with one valence electron more or less than the semiconductor. In the case of silicon, which has four valence electrons, elements with three or five valence electrons can be used. The atoms of these elements take the places of silicon atoms in the lattice structure.
If an element with three valence electrons is used for doping, it forms three valence bonds to neighboring silicon atoms, leaving one silicon atom with one bond less than usual and thus there is a hole brought into the semiconductor. Close to the lower end of the band gap, an energy level emerges, the so called acceptor level. The difference between this level and the valence band is very small. Therefore it is easy to lift electrons into it, which leave holes in the valence band that contribute to the conductivity. This is called p-doping.
Alternatively elements with five valence electrons can be used. After forming four valence bonds with neighboring silicon atoms, one excess electron per atom is left. These electrons form an energy level close to the conduction band. From this donor level they can easily be lifted into the conduction band, thus contributing to the conductivity. This semiconductors are called n-doped. Figure 2.5 shows how a phosphorous atom takes the place of a silicon atom in the lattice. An additional electron remains unbound. Figure 2.6 shows the position of the donor and acceptor levels relative to the bands and the resulting position of the Fermi level in p- and n-doped semiconductors.

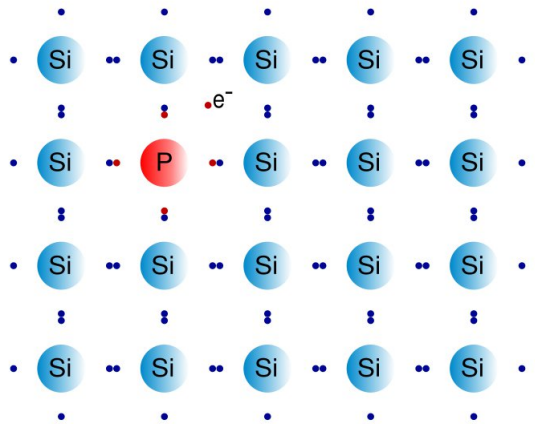

Figure 2.5.: *N-doping in silicon [Nutu]*

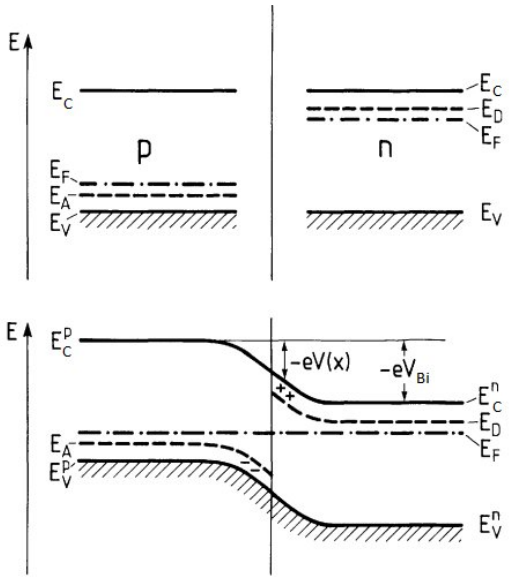

Figure 2.6.: *Schemactic of band bending in p-n-junction [Ibach09]*

There are two reasons for charge carriers to move inside a semiconductor. In equilibrium they move randomly, constantly being scattered at impurities. Therefore their effective velocity is zero. This changes under the influence of an electric field. It accelerates the charge carriers in one direction, resulting in an effective velocity; this movement is called drift.
The second phenomenon is the diffusion. It is the result of different concentration of one sort of charge carriers in different areas of the semiconductor. This induces a movement of charge carriers

from the area with the higher concentration towards that with the lower.

2.2. The p-n junction

A p-n junction develops when a p- and an n-doped semiconductor of the same element are brought in contact. The laws of thermodynamics demand that the Fermi level is constant in this system. This means that the valence and the conduction band have to bend in order to make a continual junction, as can be seen in figure 2.6. Due to the different doping there is a difference in the concentration of charge carriers in the p and n region. Naturally the concentration of holes is higher in the p region and the concentration of electrons is higher in the n region. In their respective region, they are called the majority charge carriers. The majority charge carriers diffuse from the region with the higher concentration into that with the lower. This generates an excess of the respective minority charge carriers, thus the p-region acquires negative charge, the n-region charges positively. This creates an electric field which counterbalances the diffusion. Finally, an equilibrium of the drift caused by the electric field and the diffusion occurs.
The border area between the p- and n-region is cleared of movable charge carriers by the electric field. Therefore it is electrically charged and forms a space-charge region. The size of the space-

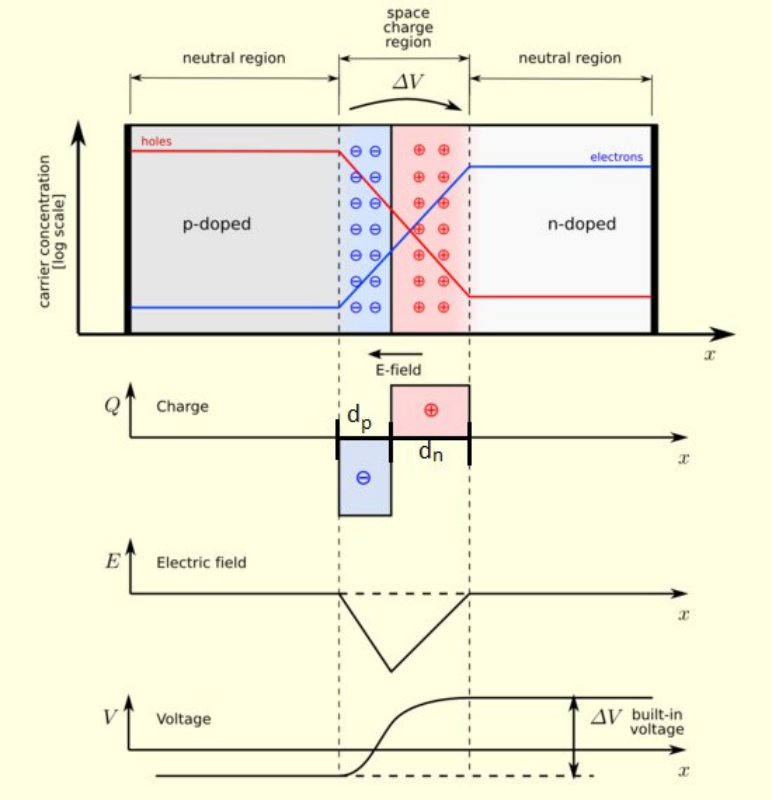

Figure 2.7.: *The structure of a p-n junction and the resulting distributions of charge, electric field and voltage [Wiki]*

charge region consists of two parts, d_p that stretches into the p-region and d_n that stretches into the n-region, as can be seen in figure 2.7. It is dependent on the concentrations N_A^- and N_D^+ of acceptor and donor atoms in the n- and p-region, the built in voltage U_{bi} caused by the intrinsic electric field of the p-n junction in equilibrium and a possible applied external voltage U [Günth 08/09]:

$$d(U) = d_n + d_p = \sqrt{\frac{2\epsilon}{q} \cdot \frac{N_A^- + N_D^+}{N_A^- N_D^+} \cdot (U_{bi} - U)}. \tag{2.2}$$

In this equation, q is the elemental charge and ϵ is the dielectric constant of the material.
The dependency on an external voltage shows the most important property of the p-n junction. In equilibrium the space-charge region prevents the junction from being conductive. Thereby the conductivity depends on the size of the space-charge region and conclusively on the external voltage.
If this voltage is positive the space-charge region shrinks, eventually allowing current to flow across the junction. The effect is caused by the external voltage that counteracts the built-in voltage and is called forward bias. When the voltage is applied in the opposite direction, called reverse bias, the space-charge region enlarges as additional charge carries are drawn out out of the center of the junction; the junction remains an insulator.
This results in an quite distinctive current-voltage characteristic. The response of the current to the applied voltage is highly non-linear, following an exponential function [Günth 08/09]:

$$I_{tot}(U) = (I^n_{gen} + I^p_{gen}) \cdot [e^{\frac{eU}{k_B T}} - 1]. \tag{2.3}$$

The currents I^n_{gen} and I^p_{gen} are the currents caused by thermal excitation of charge carriers in the n- respective p-region that diffuse into the other region in thermal equilibrium. This is illustrated in figure 2.8. The amount of charge accumulated in the space-charge region is approximately given

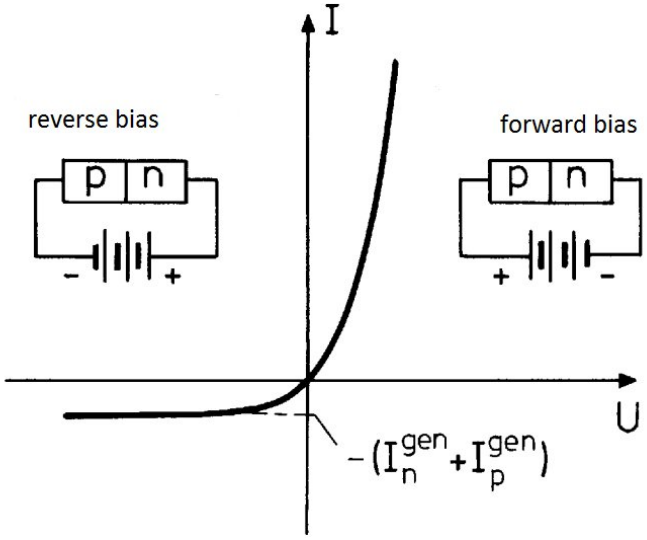

Figure 2.8.: *Current characteristic of the p-n junction [Ibach09]*

as [Günth 08/09]:

$$Q \approx eN^+_D A \cdot d(U), \tag{2.4}$$

where A is the area of the p-n junction perpendicular to the current.
The p-n junction therefore has a capacity of [Günth 08/09]:

$$C = \frac{d}{dU}Q = -e\frac{A}{2}\sqrt{\frac{N^-_A N^+_D}{N^-_A + N^+_D}\frac{2\epsilon\epsilon_0}{e(U_{bi} - U)}}. \tag{2.5}$$

2.3. The LED

One electrical component based on the p-n junction is the Light Emitting Diode (LED). As it is used in the experiment a short description of its working principles is given here.

When a p-n junction is forwardly biased, electrons and holes drift into the space-charge region. If an electron and a hole meet, they can recombine and the electron falls from the conduction band into the valence band. As this means falling into a lower energy level, the electron has to loose an amount of energy corresponding to the size of the band gap. This is shown in figure 2.9. In indirect semiconductors as silicon this happens through non-radiative transitions. Therefore they are not usable as materials for LEDs. In direct semiconductors however, the transition can be radiative and a photon with an energy equal to the size of the band gap is emitted. It is possible to adjust the color of the emitted light by choosing semiconductors with a suitable band gap. LEDs can be operated at lower voltages and consume less power than conventional light sources. They emit light in a very small wavelength region.

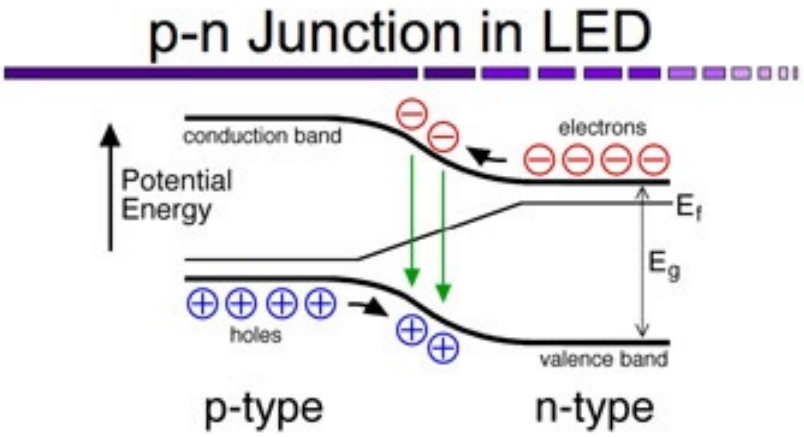

Figure 2.9.: *Emission of light in a LED [Wisc]*

2.4. The Photodiode

The photodiode is a detector that uses the properties of the diode junction to measure the presence of photons. To understand the processes that lead to a measurable signal it is necessary to look into the optical excitation of electrons in semiconductors.
When a photon hits an electron in the valence band, this electron absorbs the energy of the photon. If the energy of the photon is higher than the band gap, in the case of the direct semiconductors the electron is excited into the conduction band, and an electron-hole pair is created. If the semiconductor is indirect, an additional phonon is needed to supply the electron with the momentum needed to cross the band gap. Up to a photon energy of $3 \cdot E_g$ (size of the band gap), only one electron-hole pair is created, the additional energy is converted to thermal energy. This effect is called the inner photo effect.
Interesting for many application is the wavelength region from $400 - 800\,\text{nm}$ as it is roughly the visible part of the light spectrum. The energy of a photon with a wavelength of 400 nm is $\approx 3.1\,\text{eV}$, 800 nm correspond to $\approx 1.55\,\text{eV}$. As mentioned above the band gap of silicon is 1.12 eV. Therefore silicon is a useful material for photon detectors in this wavelength region.

This effect can be utilized in order to use diodes as photodetectors. In this case the geometry of the diode is such that photons can enter the semiconductor from one side and reach the space-charge region.
Now there are two possibilities of how the photon interacts with the semiconductor. The first one is, that the photon interacts in the space-charge region. This is the desired case because the electric field in this region quickly separates electron and hole. In order to maximize this effect

photodiodes are usually reversely biased as this enlarges the space-charge region.
The hole drifts into the p region and the electron into the n region. This is further promoted by the reverse bias. Thus they are not able to recombine and contribute to the current resulting from the incident photons. This contribution to the total current is called drift photocurrent $I_{\text{photdrift}}$.
The second possibility is that the photon interacts outside of the space-charge region. Here there is no electric field to separate electron and hole and many of the same recombine very quickly without any contribution to the current. Some on the other hand separate and diffuse into the space-charge region. This contribution to the current is called diffusion current I_{photdiff}. The total current is than simply given as

$$I_{Phot} = I_{\text{photdrift}} + I_{\text{photdiff}}. \tag{2.6}$$

As mentioned above the photons should mainly interact in the space-charge region. The absorption probability of dn of n photons while traveling the distance dx in a material is given as [Plessen]:

$$\frac{dn(x)}{dx} = -a(\lambda) \cdot n_0 \cdot e^{-a(\lambda x)} = -a(\lambda) \cdot n(x) \tag{2.7}$$

Here $a(\lambda)$ is the absorption length in the material. It is dependent on the wavelength of the incident light. Figure 2.10 shows its wavelength dependency in silicon. This causes the photodiode to be be more sensitive in some wavelength regions than in others. When designing a photodiode

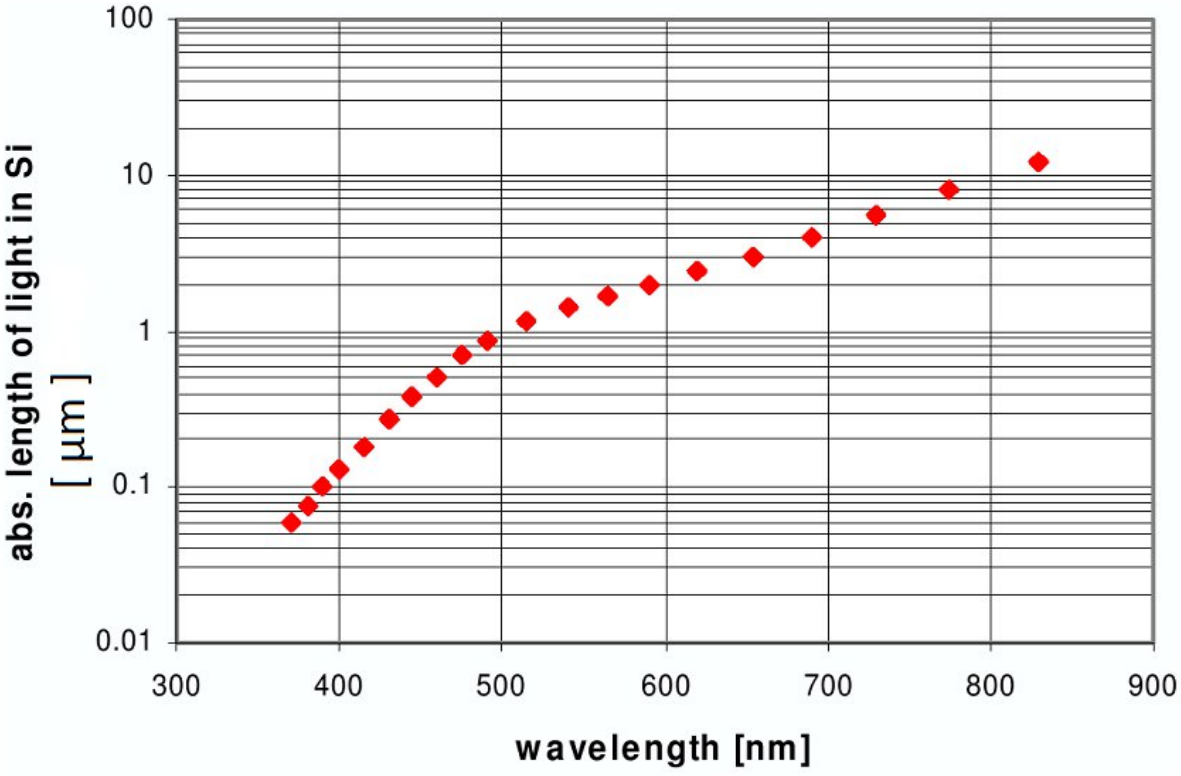

Figure 2.10.: *Wavelength dependency of the absorption length in silicon [Roper]*

the reflectivity of its surface becomes an issue. The fraction T of the light that is transmitted is dependent on the refraction index [Plessen]:

$$T = 1 - (\frac{n_1 - n_2}{n_1 + n_2})^2 \tag{2.8}$$

This equation is valid for perpendicular incidence of light. As the difference between the refractive indices of air (≈ 1) and of silicon (≈ 3.9) is very different, it is useful to add a thin layer of materials

as SiO_2 with a refraction index of 1.46 as a window. In addition, this works as a protection of the space-charge region below.

Every incident photon creates only one electron-hole pair. Therefore, a photodiode has no intrinsic gain and a large number of photons is necessary to produce a current which is high enough to be measured by amperemeters.
In consequence it is advisable to adjust the properties of the photodiode in order to increase its efficiency. To increase the size of the space-charge region an layer of intrinsic semiconductor can be placed between the p and n region. This leads to a very large space-charge-region which stretches all over the intrinsic layer and the adjacent parts of the p and n region. This design is called a PIN-diode and is a very common photon detector. Figure 2.11 gives a schematic view of the PIN

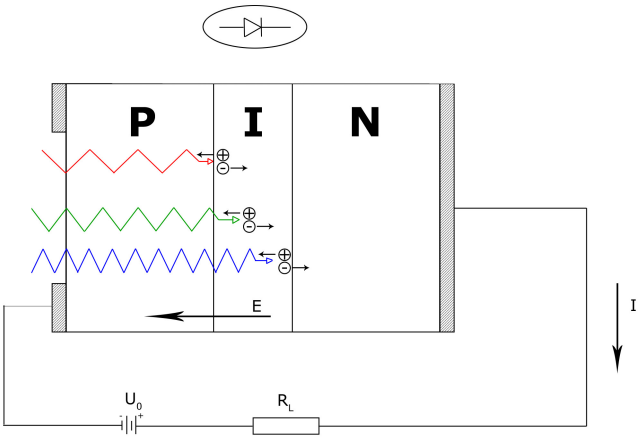

Figure 2.11.: *Structure of a PIN diode [BSSLab]*

diode. The penetration depth of the photons is wavelength dependent, indicated by the different colors of the arrows representing the photons.

2.5. The Avalanche Photodiode (APD)

To build semiconductor photon detectors with intrinsic gain the effect of avalanche breakdown is used. This requires the photodiode to be operated with a high reverse bias. The electric field in the p-n junction becomes very large, large enough to accelerate the charge carriers so that they themselves are able to ionize atoms in the space-charge region by impact ionization. Thus their kinetic energy has to be larger than the band gap. As a consequence, the number of charge carriers multiply on their way through the space-charge region, and an avalanche is created. Figure 2.12 shows the structure of such an APD. The charge carriers are created in the conversion layer and accelerated toward the multiplication layer. There they reach the energies needed for ionization. Charge carriers created in the multiplication layer itself do only cause small avalanches. If they are created even deeper within the drift layer, there is no amplification at all. This has to be considered in the design of the APD. The effect depends on the value of the applied voltage. If it is below the breakdown voltage of the diode, the signal is proportional to the number of primary charge carriers created in the conversion zone, as the holes do not contribute significantly due to their small probability of ionizing atoms. The gain that can be reached by APDs in this mode of operation is up to 10^3.
If the operation voltage is higher than the breakdown voltage the holes contribute to the avalanche too, as they are now accelerated enough to make up for the low ionization probability. This is shown in figure 2.13(a). It results in an avalanche breakdown of the diode. Each photon triggers a full breakdown and therefore the same signal. This mode of operation is called "Geiger Mode".

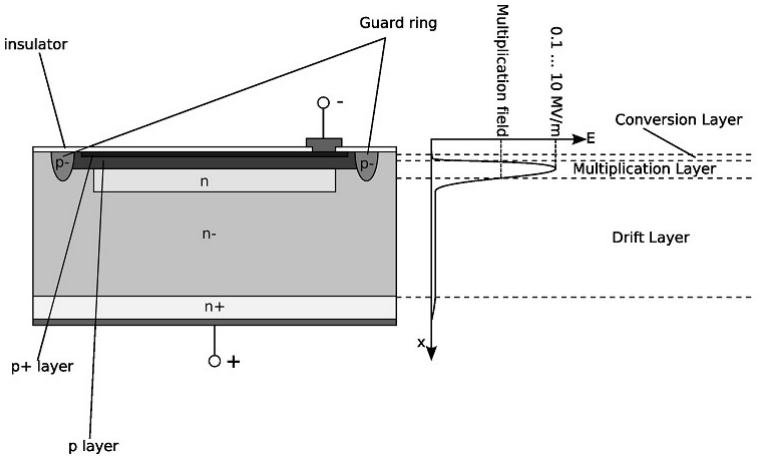

Figure 2.12.: *Structure of an Avalanche Photo Diode [Roper]*

The so created Single Photon Avalanche Diode (SPAD) can only register one photon at a time because it is not sensitive after a breakdown for about 10^{-8} s [Mos] The SPAD has a gain of up to 10^6. Another problem is that the breakdown does not stop of its own accord. Therefore a

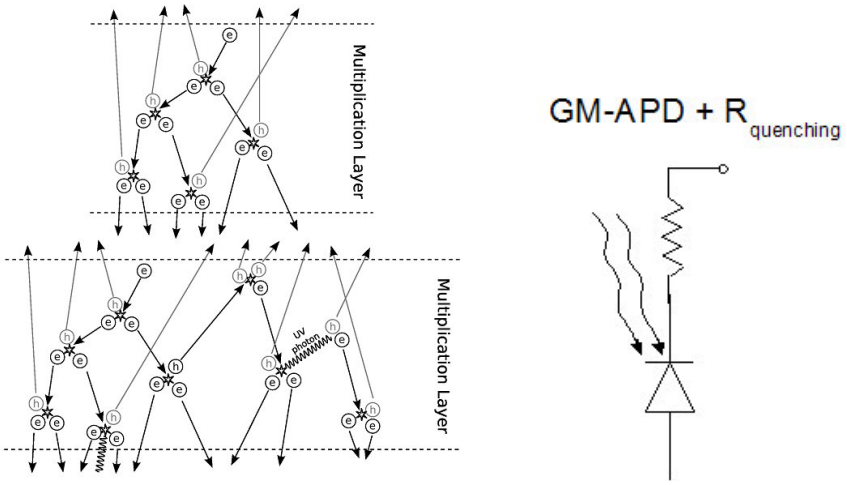

(a) Charge carrier multiplication in an APD. The upper case is below, the lower above breakdown voltage [Roper]

(b) Schematic of an avalanche photodiode in geiger mode series connected with a quenching resistor [Pisa]

Figure 2.13.: *Schematic of the multiplication and of the electrical connection of an APD*

mechanism is needed to quench the avalanche after it is registered as a signal. This is achieved by a quenching resistor, series-connected to the APD as shown in figure 2.13(b).

2.6. The Silicon Photomultiplier

The major drawback of a SPAD is the fact, that it works as a binary device, being only able to tell if they have detected a single photon or not at a time. So no information regarding the photon flux is gained. In order to enable detection of the photon flux, many SPADs are combined into a Silicon Photomultiplier (SiPM)

2.6.1. The structure of an SiPM

The SiPM (also known under various other names, for example Pixelated Photon Detector (PPD), Geiger Avalanche Photodiode (G-APD) oder Multi Pixel Photon Counter (MPPC)), is an array of SPADs that are connected in parallel to a common load as is shown in figure 2.14. Each SPAD is referred to as one pixel of the SiPM. They are grouped on a common silicon substrate. [Dol]
It is important to electrically isolate the different pixels to minimize electrical crosstalk between them, because otherwise an avalanche in one pixel could easily trigger another one in an adjacent pixel. This decoupling is done by separating the pixel with layers of polysilicon [Dol]. The electrical connection between the pixels and the load is usually done with thin layers of aluminum. This features of the structure are shown in figure 2.15.

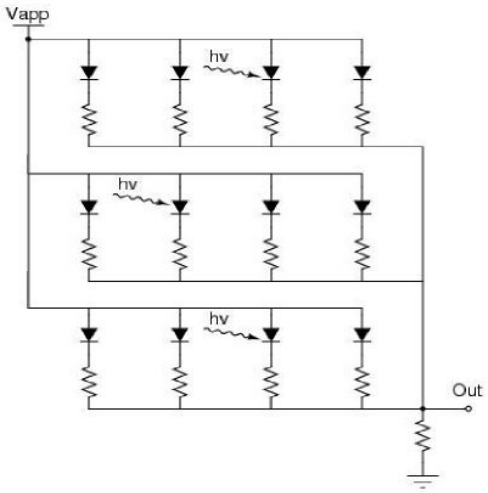

Figure 2.14.: *schematic of the connection of SiPM pixels [SensL]*

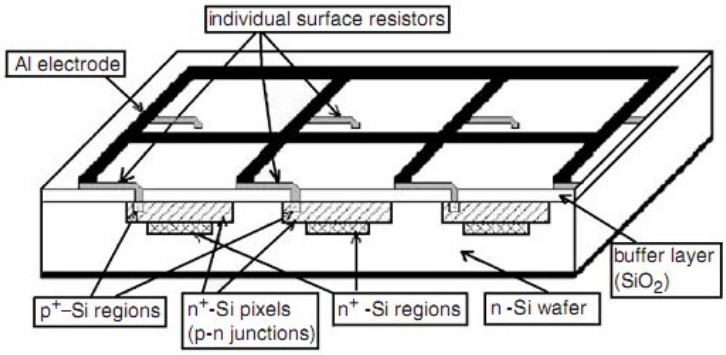

Figure 2.15.: *Structure of an SiPM [Renker]*

Because of the need to incorporate the decoupling and the quenching resistors into the design of the SiPM it is impossible to fill the whole surface of the array with active detectors. The fill factor F describes the ratio of the active area to the total surface of the SiPM:

$$F = \frac{\text{sensitive area}}{\text{total area}}. \tag{2.9}$$

The single pixel usually has a size of about $10 - 100\,\mu\text{m}$. Therefore the number of pixels per area

is typically about $10^3/\mathrm{mm}^{-2}$ [Mos]. Commercially available SiPMs often come in sizes of 1×1 or $3 \times 3\,\mathrm{mm}^2$ surface, thus providing an array of one hundred to several hundred pixels.

2.6.2. Signal and Timing

When a photon causes an avalanche in a pixel, a comparatively large current flows along the p-n junction. The time that the signal needs to rise to its full size is extremely short, at approximately 500 ps. The SiPM therefore has a very fast response. The quenching resistor prohibits the flux of new charge carriers into the junction from the outside. Only the charge carriers in the junction itself contribute to the current that is generated by the avalanche. The amount of charge is hence given by the capacity of the pixel and the difference between the operational voltage and the breakdown voltage of the p-n junction [Moser]:

$$Q = C_{pixel}(V_{op} - V_{breakdown}). \tag{2.10}$$

If this value is then set in relation to the elementary charge e, the gain of the pixel can be given as [SensL]

$$G = \frac{C_{pixel}(V_{op} - V_{breakdown})}{e}. \tag{2.11}$$

Increasing the overvoltage $\Delta V = V_{op} - V_{breakdown}$ is therefore the easiest way to increase the gain of the SiPM. Since the pixels forming one SiPM are essentially identical, each time a pixel is triggered the same amount of charge contributes to the signal that is produced by the whole SiPM. This makes it possible to combine the signal of many binary devices to a quasi-analogue signal proportional to the photon flux. The signal at the output node of the SiPM has discrete levels corresponding to the number of photons that triggered a pixel at a time. This is only possible as long as the flux is not too high. The limiting factor here is the dynamic range of the SiPM. This is the range of the number of incident photons that can be measured at a time. This properties make it possible to measure photon spectra with the SiPM with far less effort as with PMTs.

After a pixel was triggered some time is needed to recharge it. This time is called the recovery time and depends on the capacity of the pixel and the size of the quenching resistor [Moser]:

$$\tau = C_{pixel} \cdot R_{quenching}. \tag{2.12}$$

As a result of this, the pixel is unable to detect another photon during this time. As long as other pixels are ready to detect photons, the signal stays proportional to the flux. If the flux becomes higher, many pixels are not ready at the same time and the SiPM begins to saturate. Then the pixels are triggered almost all the time and the signal reaches a plateau.
Considering the recovery time of one pixel, the bandwidth of an SiPM would lie in a region of several MHz. However, as there are many other pixels that can be triggered, the effective bandwidth is much higher, converging to the value of the single pixel as the SiPM goes into saturation. [SensL].

Increasing the dynamic range requires a larger number of pixels. Accordingly the size of the pixels becomes smaller. The disadvantage of this is, that the fill factor decreases significantly as the space is needed for the many quenching resistors and the decoupling. Finding a good compromise between these two opposing properties is one of the challenges in the construction of SiPMs.

2.6.3. Noise

One of the major drawbacks of the SiPM is the high noise. At room temperature it typically is about 1 MHz. There are three contributions to the total noise of the device, random noise, afterpulsing and optical crosstalk."Random noise" is mostly caused by thermal excitation of electrons into the conduction band in the avalanche region of the pixel. Charge carriers generated by this can then cause an avalanche breakdown which contributes to the signal of the SiPM as noise."Afterpulsing" is an effect that occurs in the aftermath of an avalanche breakdown, when charge carriers, that were trapped at impurities during the avalanche, are released and cause another avalanche.

This can happen during a period of several µs after the avalanche [Renker]. "Optical crosstalk" is an effect that is connected to the avalanche itself. UV-photons can be generated by recombination of holes and electrons during the breakdown at a rate of about 3 photons per 10^5 charge carriers [Renker]. These photons can then hit another pixel and cause an avalanche breakdown. As the possibilities for these three effects are rather large, the SiPM has a high level of noise.

All effects contributing to the noise level are dependent on the overvoltage, rising with increased value of ΔV. Therefore much consideration has to be made regarding the trade off between gain and noise. Since the noise is increasing tremendously when ΔV exceeds a certain value, an optimal region for the overvoltage has to be found for each SiPM. [SensL]

2.6.4. The photon detection efficiency

For the practical use of SiPMs as a photon detector, it is absolutely necessary to know what fraction of the incident photon flux is actually detected by the SiPM. It is expressed as the Photon Detection Efficiency (PDE). This value is given as [SensL]:

$$PDE = \eta \cdot \epsilon \cdot F, \tag{2.13}$$

where η is the quantum efficiency, ϵ is the probability for a charge carrier to initiate an avalanche and F is the fill factor.
The quantum efficiency describes the probability of a photon to generate a electron-hole pair in the semiconductor. It depends highly on the wavelength of the photon because of the wavelength dependency of the penetration depth of photons in semiconductors.
For most SiPMs the peak sensitivity lies between 450 and 600 nm and drops significantly at lower wavelengths [Moser]. For wavelengths larger than 450 nm the photons penetrate deeply into the semiconductor and generate electron-hole pairs below the avalanche region. The electrons are drawn into this region and trigger the avalanches. This of course is true only for SiPMs built on a p substrate. For wavelengths between 350 and 400 nm the electron-hole pairs are generated directly below the surface of the diode above the avalanche region. Here the holes are drawn into the avalanche region. Because of their lower probability of initiating an avalanche, the sensitivity is lower in this region. This can be reversed by using an n substrate and inverting the structure of the SiPM, thus adjusting the sensitivity for different wavelength regions [Moser].

3. Experimental Setup

As the goal is to measure properties of an SiPM under monitored conditions, the setup has to comply with several requirements. Firstly it has be able to ensure the supply of the SiPM with its operation voltage and to collect the signals it generates. This signals then need to be processed properly to make them usable in data analysis. The second major task is to create an environment in which the SiPM can be exposed to a controllable and monitored amount of light.
The first obvious decision is to place the setup into a dark box to block any light from sources other than the ones used in the experiment. To monitor the amount of light that falls onto the SiPM a PIN diode is used. The premise for this to work is that it can be guaranteed that the photon flux to the PIN diode can be directly related to the one to the SiPM. This is achieved by using an integrating sphere, which is able to diffuse light that is sent into the sphere to a degree that it can be safely assumed that it is distributed uniformly in all directions.
The next section will describe all the devices used to transform this ideas into a practical setup. After that the combination of them into the setup is shown before discussing the timing and the data acquisition.

3.1. Used Devices

3.1.1. The silicon photomultiplier

Object of interest and therefore one of the most important components in this setup is the SiPM. Used is a S10362-11-100C from Hamamatsu. It has a pixel size of 100x100 μm^2 and a pixel number of 100, resulting in an effective active area of 1 mm^2. With a value of 0.785, the fill factor of the SiPM is rather large. It can be used in a temperature range from $-20 - 40\,°C$. As the experiment is performed at room temperature this will be no issue. The SiPM is sensitive in a wavelength region from 320 to 900 nm with the peak sensitivity wavelength at 440 nm. Hamamatsu states the photon detection efficiency (PDE) as 65%. As it is not discernable how this value was measured and no information about the uncertainty is given, a more precise measurement of the photon detection efficiency is necessary before it can be used as a detector in research. In figure 3.1 the behavior of the photon detection efficiency (PDE) dependent on the wavelength is shown for SiPMs of different sizes. The last numbers indicate the pixel size and the last letter the package material. Shown here are the graphs for a metal package. Used in the experiment was a SiPM with ceramic package, indicated by the C at the end of the type number. This makes virtually no difference in the behavior of the PDE. The optimal operation voltage ranges from $60 - 80\,V$, with a precise specification given for each individual SiPM by Hamamatsu. At this operation voltage, the dark count lies typically at 600 kHz with the maximum dark count ranging up to 1000 kHz.
The specific SiPM used in the experiment has an operation voltage $V_{op} = 71.31\,V$ and a dark rate of 714 kHz. As the detector was operated a 10 mV below the operation voltage, the actual dark rate in the experiment lies somewhat below this value. Terminal capacitance C_t of the SiPM is 35 pF and the time resolution lies between $200 - 300$ ps, the Gain is given as $2.4 \cdot 10^6$ [Hama1].

3.1.2. The SiPM front-end electronics

In order to measure and process the signals of the SiPM, as well as to provide the operation voltage, a front-end electronics board has been developed by F. Beißel of III. Physikalisches Institut B. It possesses a number of functions that help to measure the SiPM output in good quality.
Firstly the provision of the operation voltage. As this has to be set very accurately, the board features a potentiometer and electronics for precision adjustment. This controls the voltage directly at the point were the SiPM is soldered on and it is far more precise than adjustments at the voltage sources. To manually control the appointed voltage the board has a monitor point where it can be

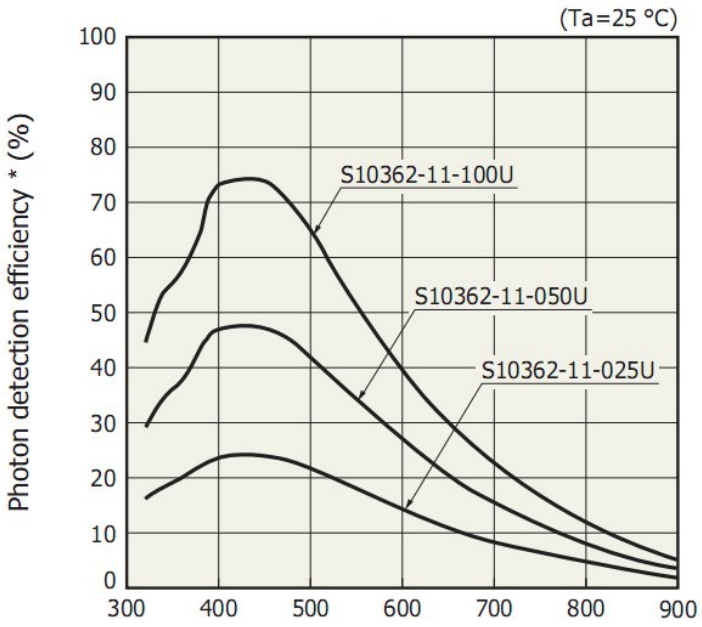

Figure 3.1.: *Wavelength dependency of the photon detection efficiency (PDE) [Hama1]*

measured with a multimeter.
The signal of the SiPM is amplified by a factor of 15 and decoupled by a 20 nF capacitor after going through a threshold that can be adjusted by another potentiometer. To connect the SiPM output to measurement devices the board holds two LEMO connectors. One of them is connected to a fast amplifier stage, the other one is connected to an integrating amplifier stage that features a 20 pF capacitor for that purpose.
The amplifiers on the board need an operation voltage of ± 5 V. All voltages and the ground are supplied via a D-SUB connector.

3.1.3. The PIN diode

As a reference detector for the photon flux a PIN diode is used. Chosen was the model S9195 from Hamamatsu, which is a rather large PIN diode with an active area of $5 \times 5\,\mathrm{mm}^2$, housed in a TO-8 metal package. While this provides a larger signal than that of diodes with smaller active areas, it also generates more noise, resulting in a dark current of about 200 pA. Figure 3.2 illustrates the reverse voltage dependency of the dark current. Additional to this information from the data sheet, the dark current was measured to have a more exact value to use in data analysis.
The maximum value for the reverse voltage is 20 V with 10 V as recommended reverse voltage in operation. The diode is sensitive in a wavelength region from $320 - 1200$ nm, with the peak sensitivity at 840 nm, as can be seen in figure 3.3. As the graph illustrates, the sensitivity in the region considered in this experiment is somewhat lower than at peak sensitivity. Nevertheless it is high enough to render a sufficient signal to noise ratio at the intensity of the light used.
The PIN diode has been calibrated by Hamamatsu. As the results of this have been documented sufficiently, the response to light of different wavelength is known well enough to use the diode as a reference for the measurements with the SiPM. The calibration data can be found in appendix B.

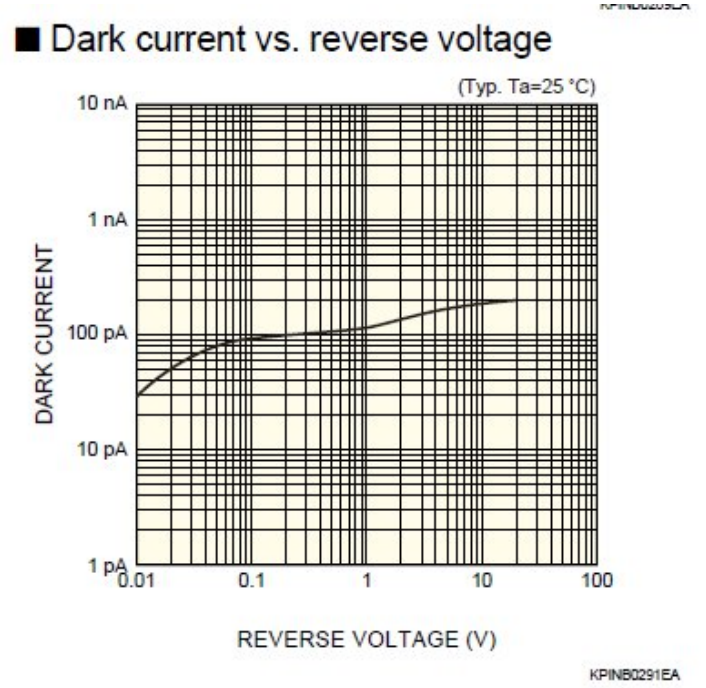

Figure 3.2.: *Dark current over reverse voltage [Hama2]*

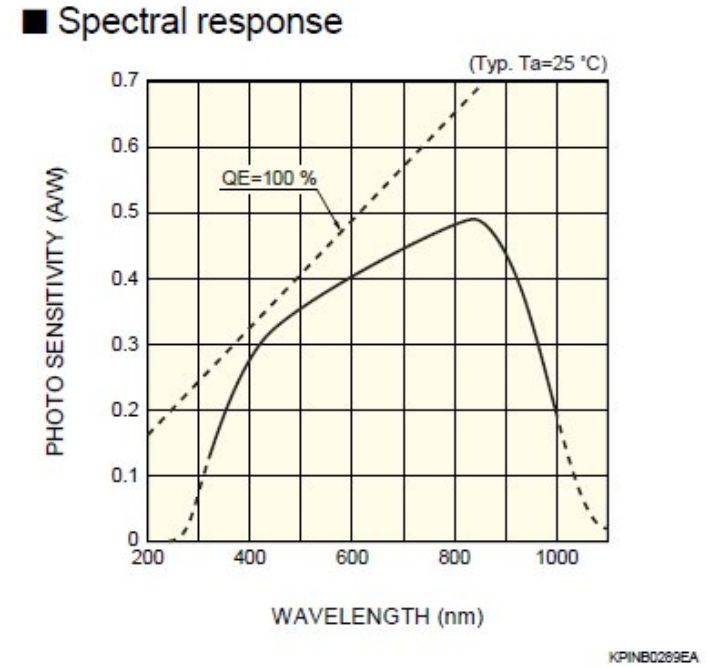

Figure 3.3.: *Wavelength dependency of photon sensitivity [Hama2]*

3.1.4. The ultraviolet LED

As a light source the L-7113UVC LED produced by Kingbright is used. It emits light with a peak wavelength of 400 nm, with the dominant wavelength at 395 nm (dominant wavelength being the wavelength perceived as the one with highest intensity by the human eye). The wavelength distribution has a half-width of 26 nm and is therefore very narrow, as illustrated in 3.4. The typical value for the forward voltage is given as 3.8 V, the maximum being 4.2 V [King]. The

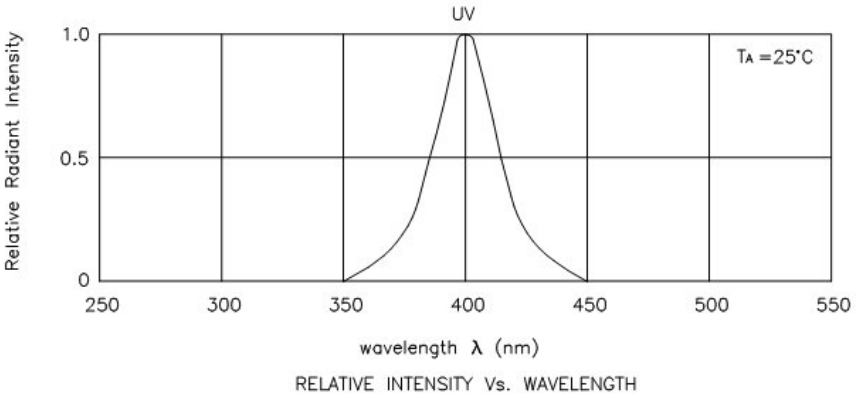

Figure 3.4.: *Wavelength distribution of the LED [King]*

geometrical properties of the LED shape the emitted light. The spatial distribution of it is shown in 3.5. As can be seen, the light is mostly emitted in forward direction.

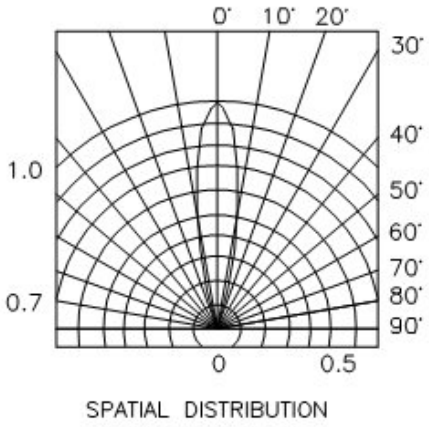

Figure 3.5.: *Spatial distribution of the LED light [King]*

3.1.5. The integrating sphere

Integrating spheres are hollow spheres coated on the inside with highly reflective materials. They have several ports to which light sources and detectors can be connected. The model used was the IS 200 from Thorlabs Inc. It is coated on the inside with polytetrafluorethylen (PTFE), better known as Teflon[1]. This material has a reflectance of approximately 99% over a large range of the wavelength spectrum, as illustrated by figure 3.6.

[1] Trademark of DuPont

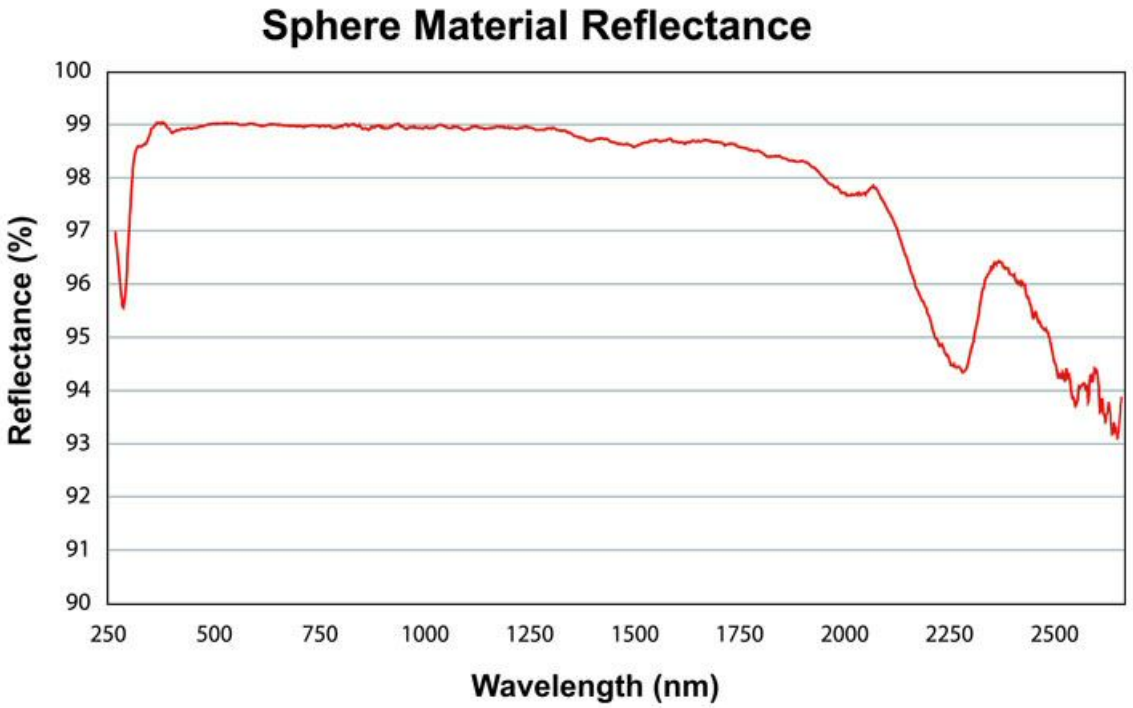

Figure 3.6.: *reflectance of the integrating sphere over wavelength [Thor]*

As can be seen in the relevant wavelength area of about 400 nm this high reflectance is reached. Therefore it can be assumed that practically no intensity is lost inside the sphere. The function of the integrating sphere is to scatter the incident light by multiple reflexion on the inside surface. Thus the light becomes diffuse and looses all anisotropy.
The sphere has a diameter of 2 inch. It has three ports with 0.5 inch diameter and a additional small port for detectors from Thorlabs. The surface area of the ports therefore is about 5% of the whole inner surface of the sphere. This in considered to be the highest fraction of non-reflective surface in the sphere that does not disturb the function as a diffusor.
To prevent the direct exposure of the ports with the light from the light source, the port dedicated for a detector is set back a little. As no detector used in the intended setup fits this port, it was not used and closed. For the assembly of the detectors additional mechanical components are needed. Some of them were purchased from Thorlabs, others were constructed and built in the mechanics workshop.

3.1.6. The picoamperemeter

To measure the output currents of the PIN diode with the precision needed it is necessary to use a extremely precise amperemeter. The PIN diode has a 25 times larger surface than the SiPM. If ten photons reach the SiPM, 250 reach the PIN diode. As the quantum detection efficiency of the PIN diode lies at approximately 80%, about 200 photons create charge carriers. At a frequency of 100 Hz this are 20000 electrons per second, corresponding to a current in the order of 10 fA. The Picoammeter 6485 from Keithley fulfills this requirements. It has a maximum resolution of 10 fA and allows external programming and data readout via a RS232 interface. The currents to be measured can be connected to the picoamperemeter via a BNC connector at the backside. Currents can be measured over a range of eight orders of magnitude, the lowest current range being up to 2 nA, the highest up to 20 mA. On each range level, the maximum current that can be measured is 5% over range. Crucial to a precise measurement is the measuring rate. It sets the time over which the current is integrated to get one current reading. It can be adjusted as the

number of power line cycles per reading. One power line cycle lasts 16.67 ms in 60 Hz mode and 20 ms in 50 Hz mode. The number can be chosen as 6 for 60 Hz and 5 for 50 Hz (SLOW), 1 (MED) and 0.1 (FAST).
Before data taking a zero correction should be made to get rid of any internal currents that could affect the measurement [Keithley].

3.1.7. The pulser

To pulse the LED a pulse generator from HP was used. Troughout this thesis it will be referred to as the pulser. It can produce pulses with a maximum height of 5.3 V and a minimum pulse width of about 2 ns. The baseline of the pulses can be shifted by 2.1 V up and down. The pulser can generate pulses up to a rate of about 10 MHz. The device is completely analog, all settings have to be done by hand. As this is rather inaccurate when it comes to the frequency, it is advisable to use an external trigger to fix a frequency from the outside. For this function the pulser has an internal delay of 18 ns fix plus an additional selectable delay of minimum 2 ns.

3.1.8. The charge to digital converter (QDC)

The signals of the two outputs of the SiPM front-ends are measured with the CAEN V965 QDC. This device converts charge to digital signals. It is equipped with 16 input channels and one gate common to all channels. All inputs are done via LEMO cables. Each channel has its own quantum to amplitude converter (QAC) which converts charge to amplitude by collecting the incoming charge in a capacitor until the gate time is over. The signal is than split in two, and passes through amplifiers, one with a gain of 1, the other with a gain of 8. As a next step in signal conversion, the two signals of a channel are multiplexed with the two of a neighboring channel, resulting in eight 4:1 multiplexes. This signals are than send to two 16 bit ADCs which convert the analogue signal to digital pulses, using a dual input range. The first accepts up to 900 pC with a 200 fC resolution, the second up to 100 pC, the resolution being 25 fC. Channels 0 to 7 seven are connected to the first ADC, channels 8 to 15 to the second. The signals of the ADCs then pass through the threshold comparator and the logic control. Finally they are stored in a Multi-Event Buffer that can save up to 32 events. From there they can be read out via VME. This structure can be seen in figure 3.8. Figure 3.7 shows the timing in the QDC. The first important period is the gate. It has to be noted that the signal to be measured has to come at least 15 ns after the gate. During the gate period an input current flows in, as shown at the top of the diagram. As a result, the output of the QAC section rises accordingly. When the gate shuts, a settling time of 600 ns follows. After that the digitization takes place, lasting about 6 µs. In this time the memory is active, writing the taken data. A clear phase follows, lasting 600 ns. Here the QDC is open for "Fast Clear" commands and the accumulated charge from the QACs drains off. Together with the gate time, typically in the range of 100 ns, the QDC takes over 7 µs for one data taking, resulting in an upper boundary of about 100 kHz for data taking frequency. Important for measurements with the QDC are the pedestals. They result from currents flowing in the QAC sections and are integrated while the gate is open. The value calculated by the QDC for the pedestal current is the value it gives out when there was no signal to detect during a gate. This pedestal is basically the signal for no photon detection of the SiPM during a gate and can be seen in the SiPM spectra if the number of photons is not too high.

3.1.9. The VME-USB-Controller

The "Wiener VM USB" is a VME[2] module that allows for PC-controlled data acquisition via an USB[3] interface. It can be used for communication with other VME modules in a crate, thus enabling the user to configure and read out those modules by software.

[2] VME (Versa Module Eurocard) is a special electronic board design format which allows for power supply and communication of different modules in one crate.
[3] USB (Universal Serial Bus) is a standard connector type for use with Computers. It allows for maximum 420 Mbit/s transfer rate in the latest version USB 2.0.

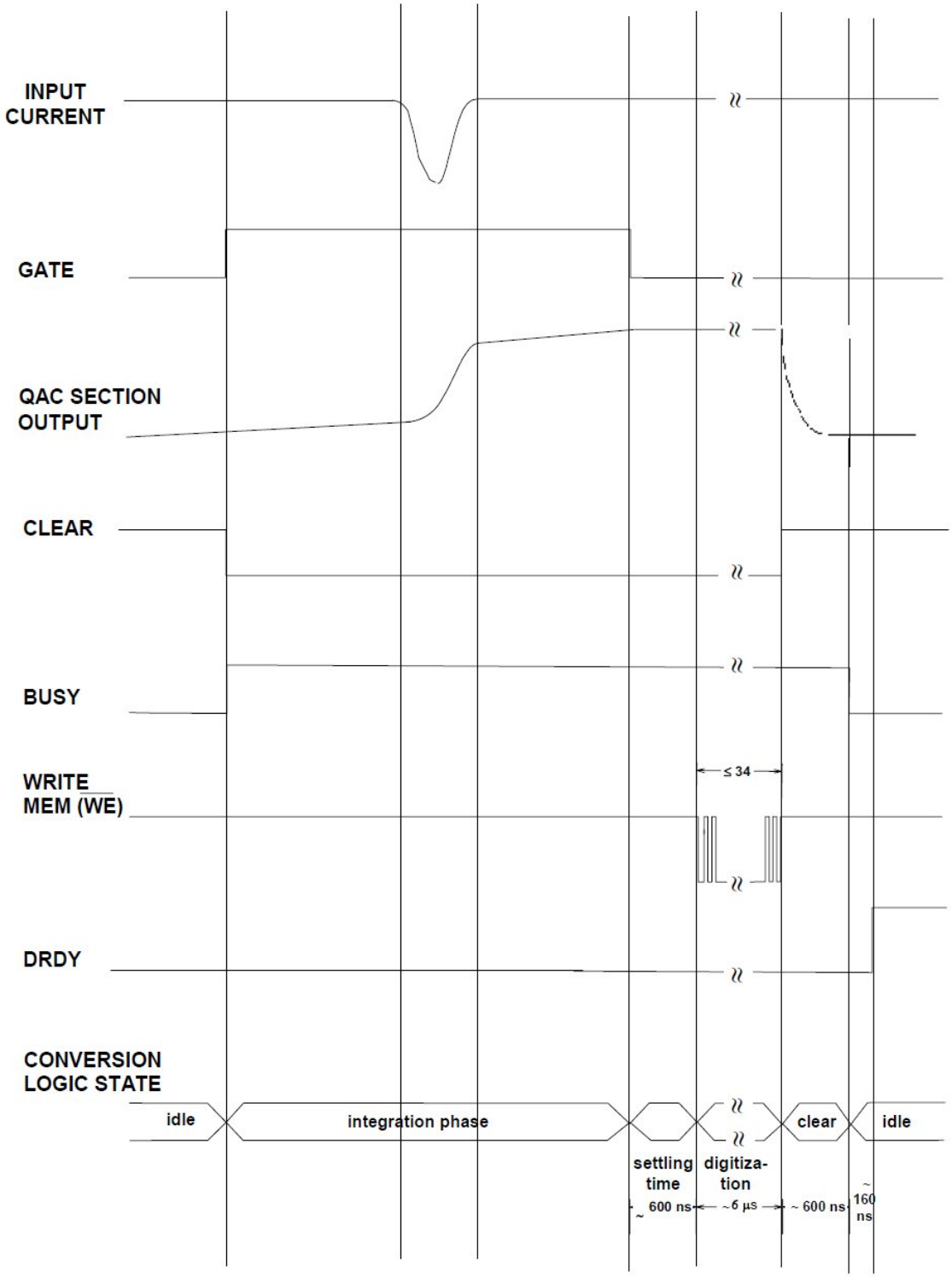

Figure 3.7.: *Timing scheme of the QDC [Caen]*

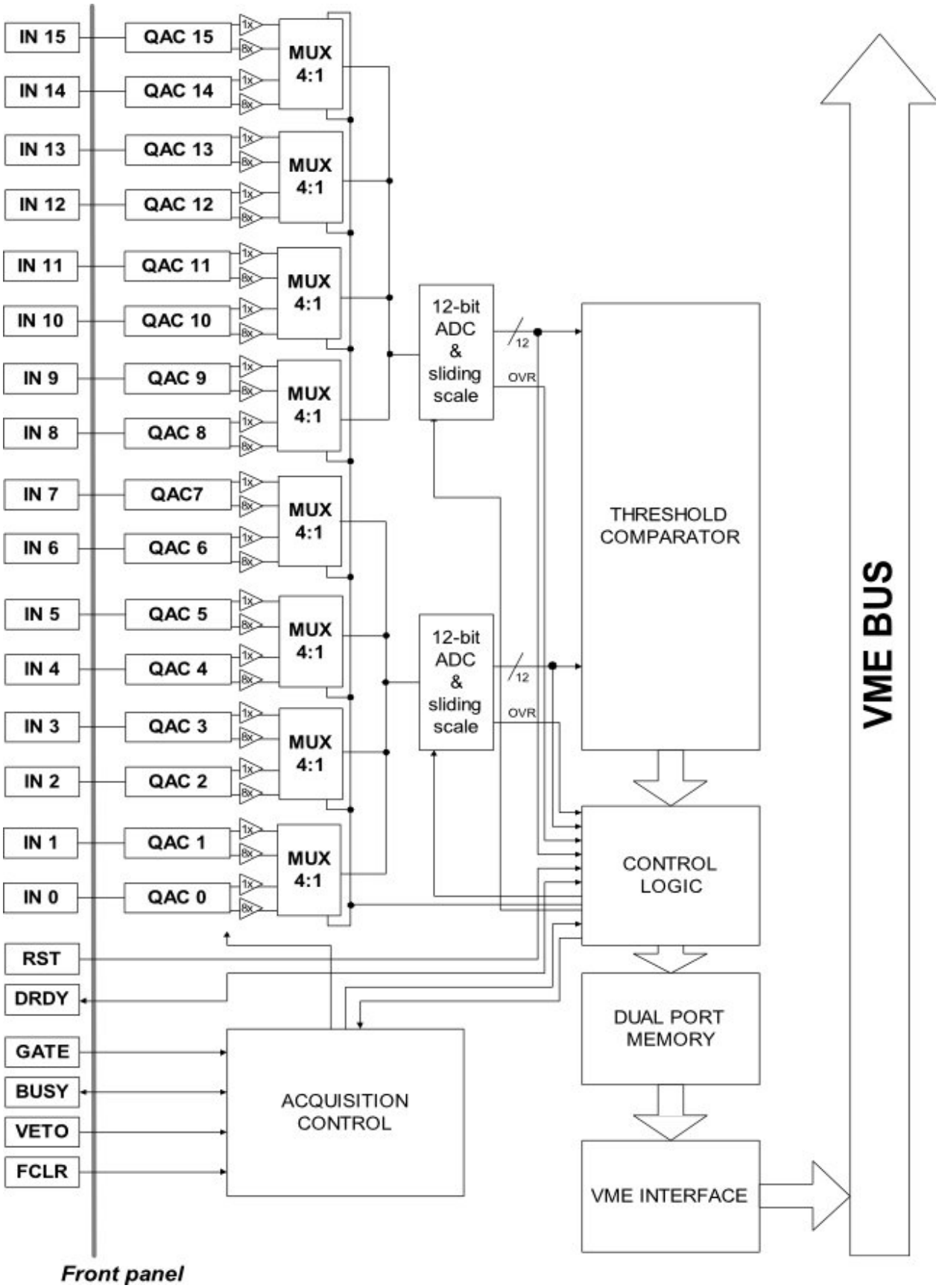

Figure 3.8.: *scheme of the signal processing in the QDC [Caen]*

Connection to the computer is established via a USB 2.0 connection. The VM USB has a programmable internal logic that can conduct the VME communication with other modules without any external control via USB necessary. The acquired Data is stored in a 24 kB Buffer.
The VM USB has 4 front panel I/O LEMO ports, accepting and sending NIM signals. To the two output ports, the signals of two independent pulse generators can be set. The pulse generators, based of the 16 MHz internal system clock, generate pulses with a width adjustable in 12.5 ns steps [Wien].

3.1.10. The oscilloscope

The Oscilloscope in this setup is a Wavejet 354 from Lecroy. It has four input channels and a bandwidth of 500 MHz. The sampling rate is 2 GS/s and shared between two channels. The sampling rate halves when more than two channels are used. The maximum capture time is 500 µs. It is possible to store screenshots and data on a USB-stick. Furthermore, operation and data readout can be done remotely via ethernet. The oscilloscope is used to measure frequency and signal properties as pulse width and height [Lecroy].

3.1.11. Other Parts

- The Dark Box
  To shield the setup from exterior light sources the light sensitive parts of the experiment are set into a dark box. It was built by the mechanics workshop of III. Physikalisches Institut A for the purpose of SiPM measurements and the described setup is the first application making full use of it.
  The box consists of a bottom panel and a lid that fit exactly together. It is made of aluminum and therefore works as a Faraday cage. This electrical shielding adds a lot to the precision of the measurements. The inside is coated with a highly non-reflective material to absorb all light that might get into the box through possible light leak. To further increase the light tightness the joints between bottom panel and light are additionally sealed with foam rubber.

- Voltage Sources
  - Peaktech 6035D Voltage Source
    This voltage source is used to provide the reverse voltage for the PIN diode. It creates voltages from $0 - 30$ V DC with a maximum current of 2.5 A. It can also provide fixed voltages: 5 V at 0.5 A and 12 V at 0.5 A. The digital display shows only one decimal place, so the accuracy of the selected voltage is only 100 mV.
  - Elektroautomatik PS 2316-050 Voltage Source
    This device has two voltage outputs. Both of them provide up to 16 V DC with a maximum current of 5 A. This device is used to provide the ± 5 V to the amplifiers on the front-end electronics of the SiPM. Again the voltage resolution is 100 mV.
  - Conrad Voltcraft plus PSP 1803
    With a range of $0.1 - 80$ V DC this voltage source provides the highest voltage used in the setup. It is used to provide the operation voltage of the SiPM. The current can be up to 2.5 A. The voltage resolution is 10 mV.

- The Patch Panel
  The Patch panel is a connection converter built by the electronics workshop. On the one side it has 9 connectors for banana plugs. On the other side it has four connectors for 9-pin D-SUB cables. The nine inputs from the banana cables are connected to the nine pins of the D-SUB connectors, the four D-SUB outputs are identical.

- FAN-in-FAN-out
  This NIM module distributes an input signal in up to eight outputs identical with the input.

- Delay
  This device delays signals by using cables of the required length to reach the selected delay value.

3.2. The setup

This section will describe how the different parts are put together in one experimental setup. A schematic of it can be found in figure 3.9 The light sensitive parts of the setup are placed within

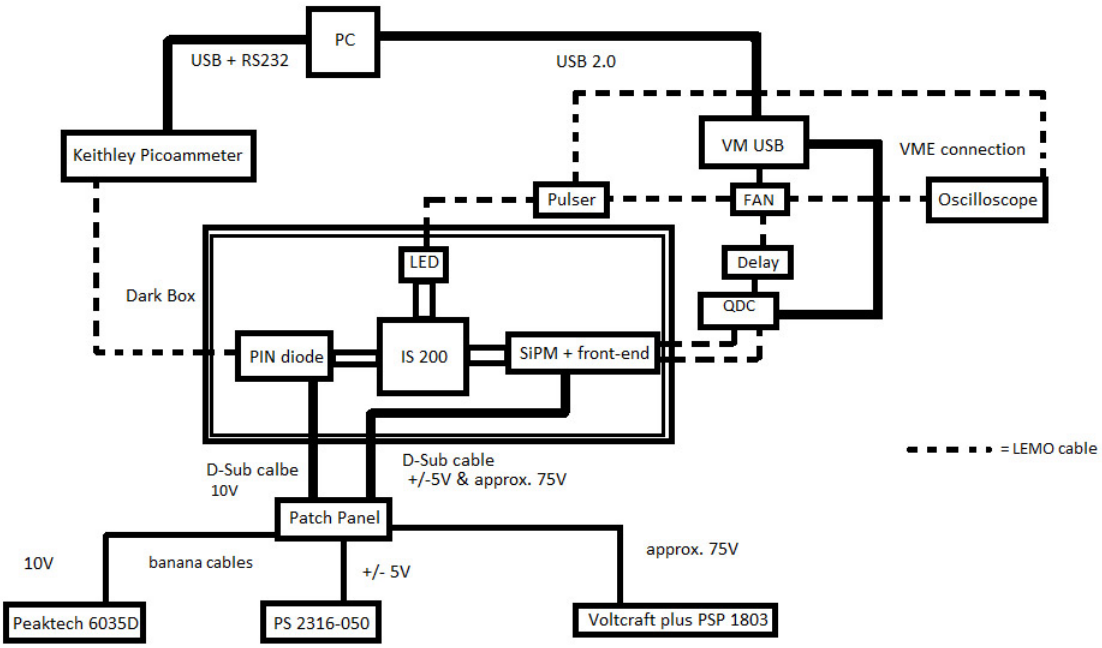

Figure 3.9.: *Schematic of the setup*

the dark box. The PIN diode, the SiPM and the LED are mounted to the three ports of the integrating sphere. As it is desirable to have only light collimated directly on the detectors to reach them, they are set back with 1 inch long tubes. To the ends of this tubes the PIN diode and the SiPM are mounted with adapters made by the mechanics workshop. Before the SiPM an additional adjustable iris diaphragm is placed which is adjusted such, that only the active area of the SiPM is visible trough it. This is done to further collimate the light onto the detector.
The LED is mounted to the integrating sphere with an adapter purchased from Thorlabs. As the two detectors do not have standard measurements no adapters for them were available and had to be built here.
The SiPM is soldered onto a front-end board which is attached to the adapter that holds the SiPM with an customized retainer, again built by the mechanics workshop.
For the LED and the PIN diode simple connector boards have been made. For the LED it holds a LEMO connector to plug in the input pulses and a connector for the pins of the LED. In a later version a 50 Ω resistor was added for termination. This was done because it was noticed that the pulse heights used in the first measurements should have been too low to trigger light emission from the LED. The explanation for this is, that the LED acted light an open end of the LEMO cable. The pulses were reflected with a phase difference and could interfere positively. Thus the signal become high enough to trigger light emission. As this behavior is unwanted, the termination was implemented.
For the PIN diode, the board has a D-SUB connector to provide the reverse voltage, a LEMO

connector for the current measurement and a connector for the pins of the PIN diode.

The SiPM and the PIN diode need operating voltages. These are provided with D-SUB cables through the trough-puts of the dark box. As the voltage sources all have outputs with banana plugs, the patch panel is needed to lay the different voltages to the pins of the D-SUB connectors. We provide the 10 V reverse voltage for the PIN diode, ±5 V for the front-end electronics and 75 V for the SiPM operating voltage. This value is larger than the real operation voltage of the SiPM, but the front-end electronics stabilize the voltage at the preset value.

The VM USB is controlled and read out by the PC via USB. The signal of its pulse generator are given to a FAN-in-FAN-out to split the signal. From there it goes on the one hand directly to the pulser via a LEMO cable where it works as an external trigger. The pulses generated by the pulser on basis of the trigger are given to the LED, again via LEMO. On the other hand the signal of the pulse generator is put through a delay and then sent to the QDC as a gate signal.

The signal output of the PIN diode is connected to the picoamperemeter via a LEMO cable. The picoamperemeter is connected to the PC with a USB cable which is plugged to the RS232 port of the Keithley with an adapter. The two output channels of the SiPM front-end board are connected to channel 0 and 8 of the QDC, again with LEMO cables. This channels are chosen because they are connected to different ADCs inside the QDC. This leads to a better readout performance than using channels connected to the same ADC. Figure 3.9 shows a schematic view of the setup. In Figure 3.10 a picture of the integrating sphere with the PIN diode, the LED and the SiPM is mounted to it and all cables plugged in is shown.

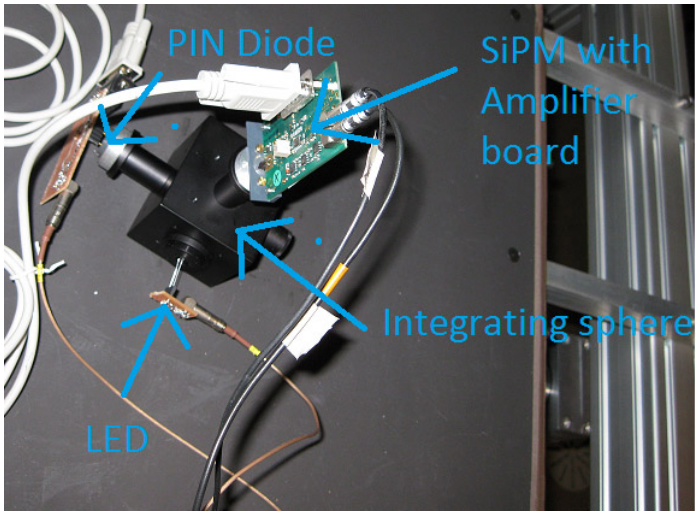

Figure 3.10.: *Picture of the setup inside the dark box*

3.3. The timing

The signals of the SiPM can only be measured by the QDC if they reach it during the gate time. Therefore it is necessary to consider the time that the signals need to travel through cables and devices in the setup. For the most part this time is caused by the cables. The signals run through the cables with about 19.7 cm/ns [Herten], so it takes a signal about 5 ns to travel 1 m.
Two important delays come on the one hand from the pulser, on the other hand from the time it takes to emit light from the LED and for the SiPM and its front-end electronics to convert it into a signal. This time is estimated as about 15 ns. The pulser has an adjustable delay with a minimum value of 2 ns plus a fixed delay of 18 ns. As the minimal delay is selected, the pulser accounts for

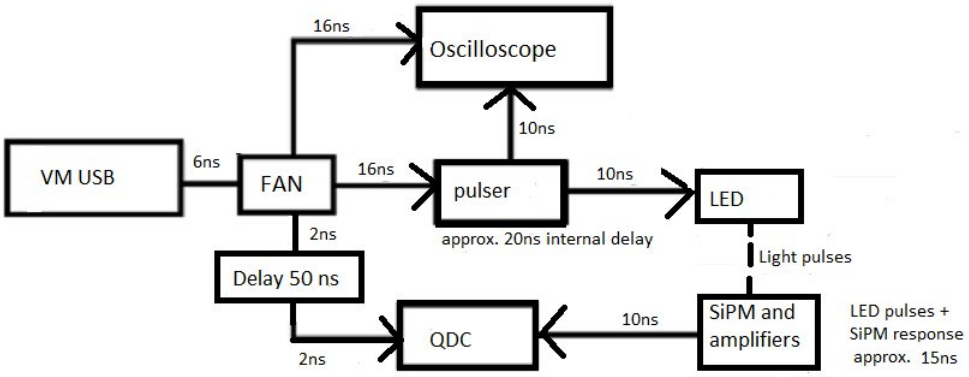

Figure 3.11.: *The timing in the signal propagation*

20 ns of signal delay.
To calculate the time difference between the gate and the signal at the QDC, the contributions along the respective signal lines have to be added up. Figure 3.11 illustrates the times that the signals needs to propagate through the cables and devices. Adding up the contributions of the different parts the direct line to the QDC takes $t_1 = 10\,\text{ns}$ while the line over the pulser and the SiPM takes $t_2 = 77\,\text{ns}$. This gives a difference $\Delta t = t_2 - t_1 = 67\,\text{ns}$.
To ensure for the SiPM signal to lie within the gate at the QDC, the gate signal is delayed with a physical delay. After comparing gate signal and SiPM signal with the oscilloscope a delay time of 50 ns is chosen. This causes the SiPM signal to arrive at the QDC 17 ns after the gate, which fits the 15 ns distance that the signal should have from the gate as mentioned in 3.1.8.

3.4. The data acquisition

The signals of the PIN diode and the SiPM are measured by the picoamperemeter and the QDC, respectively. Both of these devices are connected to a PC, the picoamperemeter via USB and a USB-to-RS232 converter and the QDC via USB.
To perform an automatic data taking, a C++ program has been written. It can vary the frequency of the pulse generator in the VM USB, thus controlling the amount of light sent out by the LED. The main data taking procedure is a loop over 14 frequencies ranging from 100 Hz to 100 kHz. Each cycle consists of three readouts. At first 100 current readings of the picoamperemeter are collected and stored in a ROOT histogram. Then 250000 QDC events are taken. They are interpreted by the software and stored in four different histograms, high and low range for each of the two channels. As a third step another 100 current readings are taken and stored in a histogram.
This additional collection of current data is mandatory because of the long duration of the QDC data taking. The QDC is not able to provide events with a frequency higher than 1000 Hz, a more realistic estimation would be 800 Hz. Therefore 250,000 events result in a measurement duration of at least 250 seconds.
It is therefore necessary to measure the current before and after the QDC data taking to check for any systematic effects that could occur during this time.

The main loop is preceded by two noise measurements. As a first step the thermal noise of the SiPMs is measured with the QDC while the LED is inactive and no light is sent into the integrating sphere. Because of the impossibility to synchronize the two pulse generators in the

VM USB properly, it is not possible to independently produce a trigger for the pulser and a gate for the QDC. Therefore one has to physically unplug the external trigger at the pulser before and replug it after this noise measurement. The data from the QDC is again stored in four histograms. The second noise measurement is done to get the baseline noise of the PIN diode. As it produces a quite large signal due to thermal excitation, this has to be measured and taken into account in the data analysis. Therefore 100 current readings are taken and stored in a histogram for further analysis.
All histograms created during the the data taking run are stored in a tree and this tree alongside with the histograms themselves is saved in a ROOTfile when the program ends.
To examine the response of the SiPM when exposed to different intensities of light, the output of the LED has to be varied. This is done by changing the height of the pulse provided by the pulser. To have the highest range possible available the offset of the pulse height is used. The baseline of the pulser is set directly below the operation point of the LED. Therefore even tiny pulses should be sufficient to initiate light emission by the LED. In reality, the pulses are so short that still a very large pulse height is needed to trigger photon emission.
With higher pulses the number of emitted photons rises accordingly. Measurements were made at three different pulse heights, each time running the aforementioned data taking routine. The properties of the pulse, mainly pulse height and width had to be taken manually from the oscilloscope. The readout of the oscilloscope via ethernet is, as mentioned above, possible, but as the implementation of its function was not completed when the measurement was done this functionality could not be used.

For the quality of data taking one important factor is the size of the gate at the QDC. Here, a compromise had to be found between cutting away part of the SiPM signal when the gate is short and admitting too much noise when it is long.
To test the influence of this setting on the QDC data, three different gate widths were chosen and the complete data taking procedure with the three different pulse heights is done for each of them. The gate width was later changed to 100 ns as a result of the analysis of the first data. Also the considered pulse heights changed after the termination resistor on the connector board of the LED was built in.

4. Analysis and Results

The first measurements with the full setup were made with gate widths of 25 ns, 50 ns and 75 ns at pulse heights of 2.7 V, 3.0 V and 3.3 V. After the implementation of the termination resistor on the connector board of the LED, the pulse heights were not high enough to operate the LED any more. Therefore the pulse heights were changed to 4.5 V, 4.75 V and 5.0 V. For this measurements also the gate widths was changed to 100 ns, based on the results of the measurements before. While most of the analysis shows the results of the later measurements, at some points data taken at the old settings is used when it was assumable that the result would not differ from the new measurements or effects of the gate widths are discussed. As a last general remark the pulse properties for all the measurements whose results are shown below are listed in table 4.1

Pulse height [V]	Half width [ns]	offset [V]
2.7	3.1	0.645
3.0	3.2	0.645
3.3	3.4	0.645
4.5	3.3	1.0
4.75	3.2	1.0
5.0	3.2	1.0

Table 4.1.: *pulse properties of all measurements*

4.1. Voltage-Current Characteristics of the LED

To have a better understanding of the LED response, the current flowing through it depending on the applied forward voltage is measured. Used for this were a Peaktech multimeter for the measurement of the voltage and the picoamperemeter for the current. The values of both devices were read off manually.The result of the measurement is shown in figures 4.1 and 4.2. In the upper

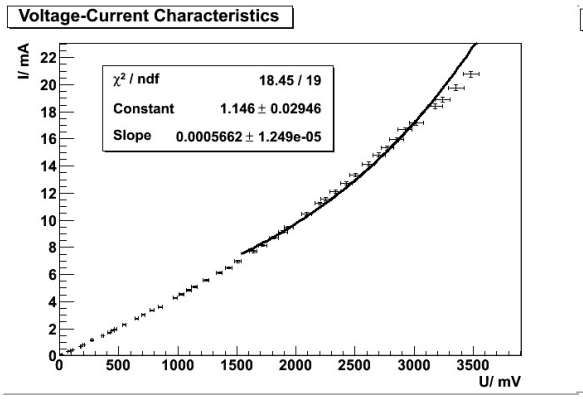

Figure 4.1.: *Current-Voltage characteristics of the LED with an exponential fit to the upper part of the curve*

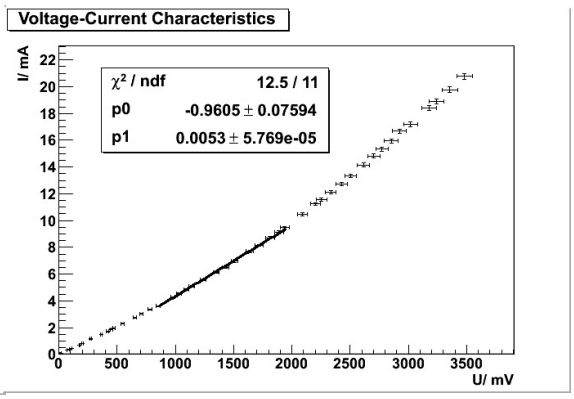

Figure 4.2.: *Current-Voltage characteristics of the LED with a linear fit to the middle part of the curve*

part, the curve follows an exponential function, in the middle the behavior is rather linear. The transition between those behaviors occurs between 1.5 V and 2 V. This reaction of the current in this voltage areas was expected and complies with the diode characteristics in figure 2.8. This

measurement was done to check if the LED behaves as expected. For the actual measurements it was operated with pulses that had a half-width of about $3.0 - 3.5\,\mathrm{ns}$. These are so short that the high pulses pose no thread to the LED as the current flows not long enough to cause any damage.

4.2. Front-end electronics noise and gain

As all electronic devices, the front-end electronics used to amplify the SiPM signal produce a noise signal. For the largest part this is white noise caused by the random movement of electrons in the circuits. For the use as a highly sensitive detector, the noise of the front-end electronics has to be quantified.
To measure the noise levels under different conditions, the two outputs of the front-end electronics are connected to the oscilloscope. The width of the noise is measured using the cursors of the oscilloscope and reading the value manually. Additionally, the wave is saved as a text-file that can be analyzed by software. Figure 4.3(a) shows the noise of the front-end electronics with no voltages

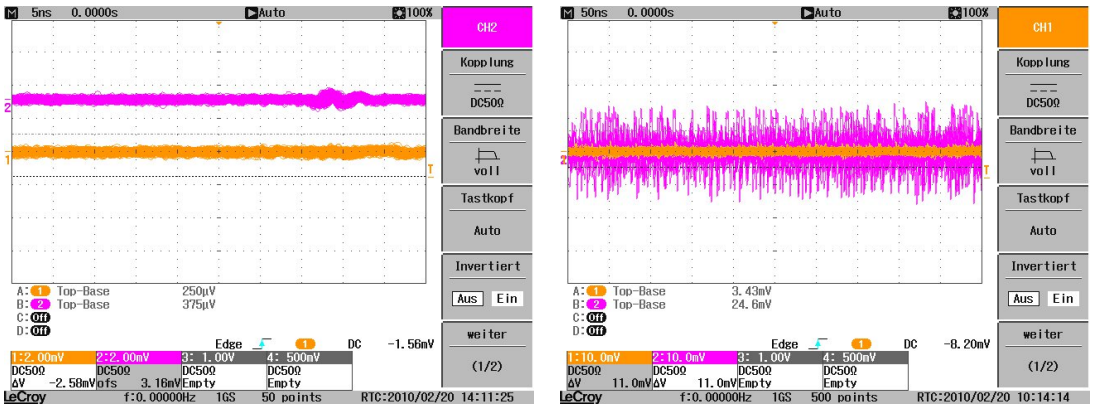

(a) Noise of the front-end boards with no voltages applied

(b) Noise of the front-end electronics at ±5 V amplifier voltage and without SiPM operating voltage

Figure 4.3.: *Pictures of amplifier noise taken from the oscilloscope*

applied. The signal of the integrating output is shown in yellow, the one of the fast in pink. Figure 4.3(b) shows the two outputs at ±5 V amplifier voltage and without the SiPM operating voltage. It can clearly be seen that the noise level of the fast output is about six times as large than the one of the integrating output. Also it can be seen that the noise fluctuates around zero, as it is expected.
The data taken from the oscilloscope is processed with ROOT and filled into histograms. Table 4.2 shows the mean and the RMS from this histograms for the different voltages and the two outputs (integrating and fast) of the amplifiers that were examined. With the exception of the

Applied Voltages [V]	Mean Int [V]	RMS Int [V]	Mean Fast [V]	RMS Fast [V]
0	$7.7 \cdot 10^{-6}$	$2.0 \cdot 10^{-4}$	$1.2 \cdot 10^{-4}$	$1.6 \cdot 10^{-4}$
±4.5	$5.8 \cdot 10^{-5}$	$4.7 \cdot 10^{-4}$	$-4.9 \cdot 10^{-4}$	$1.1 \cdot 10^{-3}$
±5.0	$1.8 \cdot 10^{-4}$	$3.5 \cdot 10^{-4}$	$-5.2 \cdot 10^{-4}$	$1.1 \cdot 10^{-3}$
±5.5	$3.1 \cdot 10^{-4}$	$5.5 \cdot 10^{-4}$	$-2.2 \cdot 10^{-4}$	$2.4 \cdot 10^{-3}$
±5.0 and 65	$1.6 \cdot 10^{-3}$	$4.4 \cdot 10^{-3}$	$-2.3 \cdot 10^{-2}$	$1.8 \cdot 10^{-2}$
±5.0 and 75	$2.3 \cdot 10^{-2}$	$7.9 \cdot 10^{-3}$	$-2.66 \cdot 10^{-2}$	$0.02 \cdot 10^{-2}$

Table 4.2.: *Means and RMS of noise levels from the saved data*

value at 5.5 V from the integrating output in can be seen that the absolute value of the mean rises

with higher voltages. Also the values of the RMS rise, which was expected because the applied voltages cause more movement of the electrons. Interesting is the fact, that the noise levels from the integrating output have positive means and the ones from the fast output have negative. This is a serious issue because the QDC does not tolerate positive input voltage higher than 15 mV without risking damage to the input stages [Caen]. As this value is exceeded by the integrating output when all voltages are applied, this output should better not be used with the QDC. But as this was done for a long time before the noise measurement without damaging the QDC, it can be concluded that the device is not as delicate as described in the manual.
As an example the histograms of the noise at 0 V amplifier voltage and without SiPM operation voltage and with ±5 V amplifier voltage and full 75 V SiPM operation voltage are shown for both outputs. For the integrating output, they can be found in the figures 4.4 and 4.5. The histograms for the fast output are shown in the figures 4.6 and 4.7. The width of the noise signal as manually taken from the oscilloscope can be found in table 4.3.

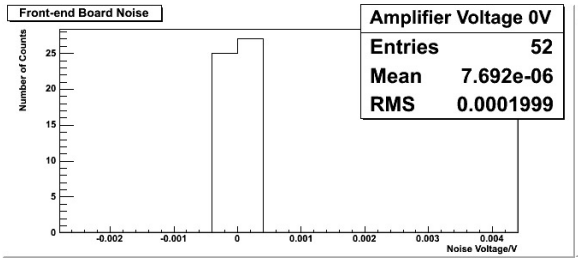

Figure 4.4.: *Noise of the integrating output at* 0 V *amplifier voltage and without SiPM operation voltage*

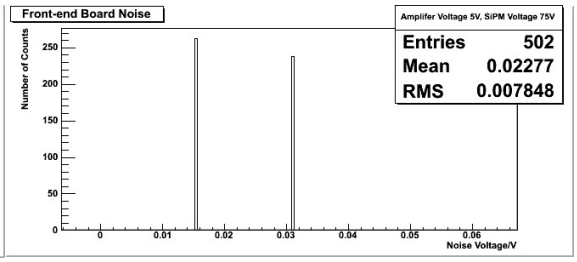

Figure 4.5.: *Noise of the integrating output at* ±5 V *amplifier voltage and with* 75 V *SiPM operation voltage*

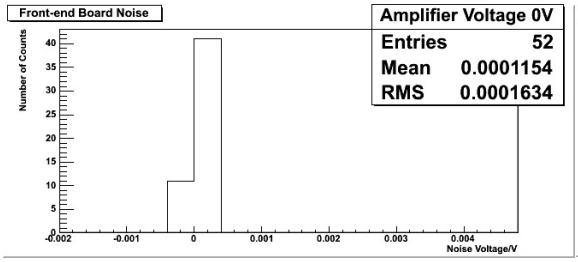

Figure 4.6.: *Noise of the fast output at* 0 V *amplifier voltage and without SiPM operation voltage*

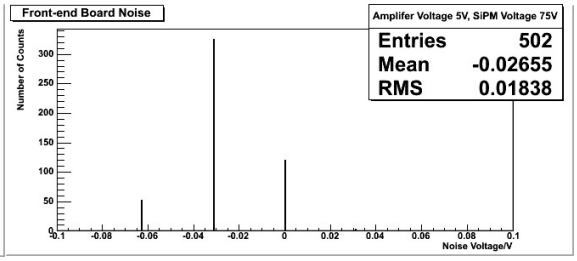

Figure 4.7.: *Noise of the fast output at* ±5 V *amplifier voltage and with* 75 V *SiPM operation voltage*

Applied Voltages [V]	Width Int [V]	Width Fast [V]
0	$1.3 \cdot 10^{-3}$	$1.5 \cdot 10^{-3}$
±4.5	$5.0 \cdot 10^{-3}$	$30.4 \cdot 10^{-3}$
±5.0	$6.0 \cdot 10^{-3}$	$32.0 \cdot 10^{-3}$
±5.5	$6.3 \cdot 10^{-3}$	$34.5 \cdot 10^{-3}$
±5.0 and 65	$5.5 \cdot 10^{-3}$	$31.2 \cdot 10^{-3}$
±5.0 and 75	$312 \cdot 10^{-3}$	$312 \cdot 10^{-3}$

Table 4.3.: *Width of the noise levels of both SiPM outputs*

The noise level with full SiPM operation voltage is of course very large, because it incorporates the actual SiPM noise signal that is discussed later.
Another important property of the front-end electronics is the gain of its amplifiers. Especially

the behavior of the gain at different frequencies is of great interest, as the frequency is varied over a large range in the measurements. To measure the gain, a capacitor with 44 pF capacity is used to couple pulses of different frequencies into the board at the contacts where the SiPM can be soldered on. The pulses were generated with the pulser and the response of the amplifiers was measured on the oscilloscope. The heights of the input signal was varied from 10 mV to 100 mV and the frequency range examined was 1 kHz to 1 MHz. The result of the measurement is shown in figure 4.8. The values were obtained by applying a linear fit to the data taken at each frequency.

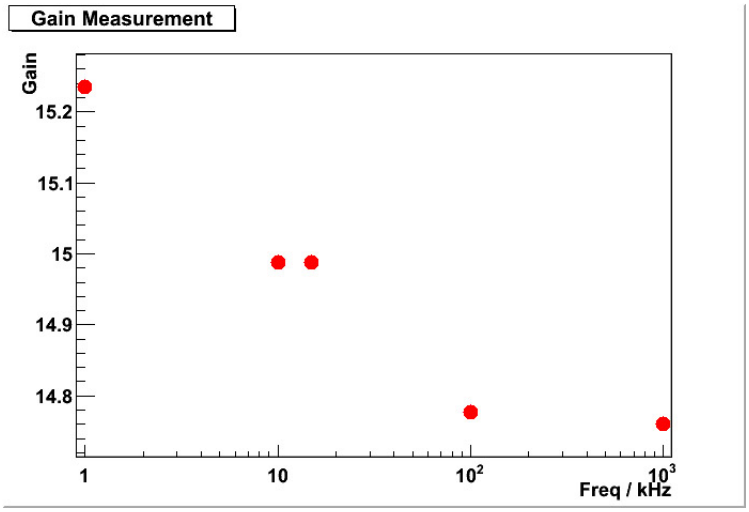

Figure 4.8.: *Results of the gain measurement*

The errors of the values obtained by this fits are so small, that they are not visible in figure 4.8 because the markers of the values had to be enlarged for better visibility. The gain is stable over the examined frequency range with a fluctuation of the values lower than 3%. This measurement was not done for the exact front-end board used in the actual setup, but as they are basically identical it can be assumed that the behavior is the same for all of them.

4.3. PIN diode baseline

Due to thermal excitation of charge carriers in the p-n-junction, the PIN diode has a considerably large dark noise. This dark noise is dependent on the applied reverse voltage, as this voltage determines the strength of the electric field in the p-n-junction and hence the probability that charge carriers are separated and contribute to the current after their excitation.
To understand the behavior of the PIN diode, it is important to measure this dependency of the PIN diode's dark current from the reverse voltage. For this measurement the reverse voltage was varied from 0 V to 12 V in steps of 0.5 V. The resulting current was measured with the picoamperemeter. Figure 4.9 shows the behavior of the dark current over the reverse voltage. The current approaches a plateau at about 700 pA. At 10 V, the voltage used during the measurements, the value for the dark current lies at $(661.00 \pm 0.52) \cdot 10^{-12}$ A. As this value might vary with time, especially under the influence of temperature, the baseline is repeatedly determined at each data taking run. The region around 10 V is appropriate for measurements because the impact of voltage fluctuation is much lower than at lower voltages. In the datasheet, Hamamatsu gives a value of 200 pA for the baseline at 10 V bias voltage. The fact that the measured value lies so much about this can be explained by the non-perfect condition under which the measurement took place, for example no temperature control and no exclusion of electric fields.

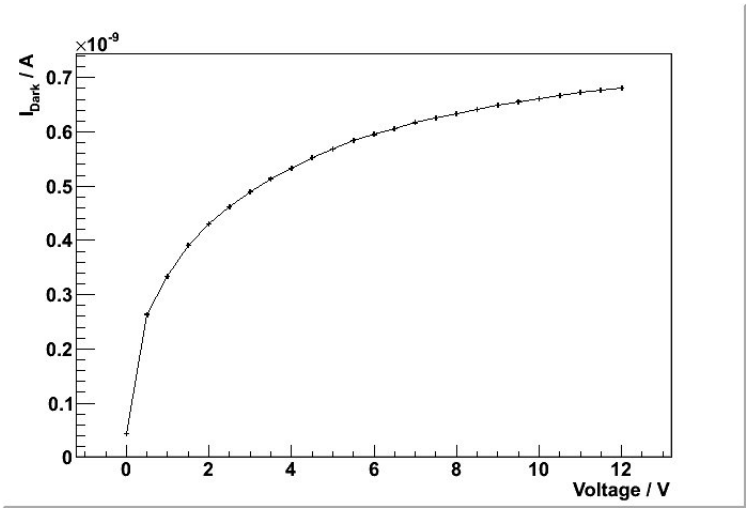

Figure 4.9.: *Dark current of the PIN diode over applied reverse voltage*

4.4. SiPM Noise

Most interesting in this analysis is of course the signal of the SiPM. At first, the noise of the detector has to be considered. It is useful to take a look at the output of the front-end electronics with amplifier voltage and SiPM operation voltage applied. Figure 4.10 shows the signals on the oscilloscope. The signal from the integrating output is displayed in yellow(the signal on top), the one of the fast output in pink(the signal at the bottom). The difference in the shape of the signals can easily be seen. The integrated signal is much rounder. This shifts the peak of the signal by a few nanoseconds, which is why the other output is called "fast". The shape of the signal is typical

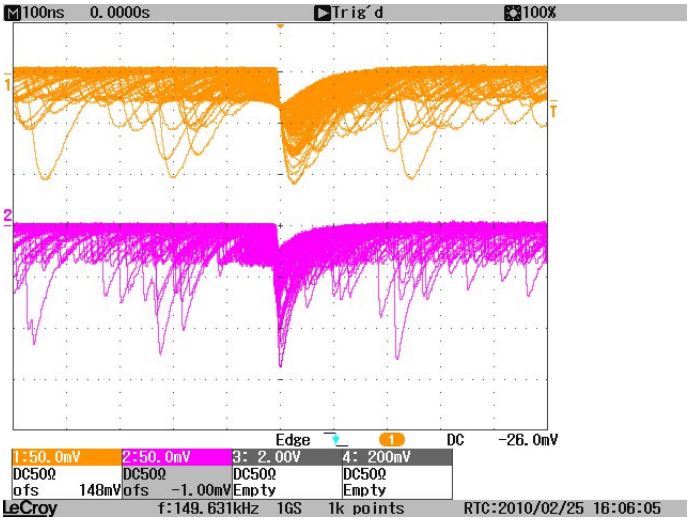

Figure 4.10.: *Signals of the two SiPM outputs*

for the SiPM. The steep falling edge shows how fast the avalanche in the triggered pixel is built up. When the avalanche is quenched the signals run out in a long tail. This becomes even clearer when taking a look at figure 4.11, where the persistence time is set to infinity and the oscilloscope's display mode is set to spectrum. The measured frequency of the noise pulses lies at about 650 kHz. This is significantly lower than the value of 714 kHz given by Hamamatsu and is due to the fact,

that the SiPM was operated 10 mV below its operation voltage.

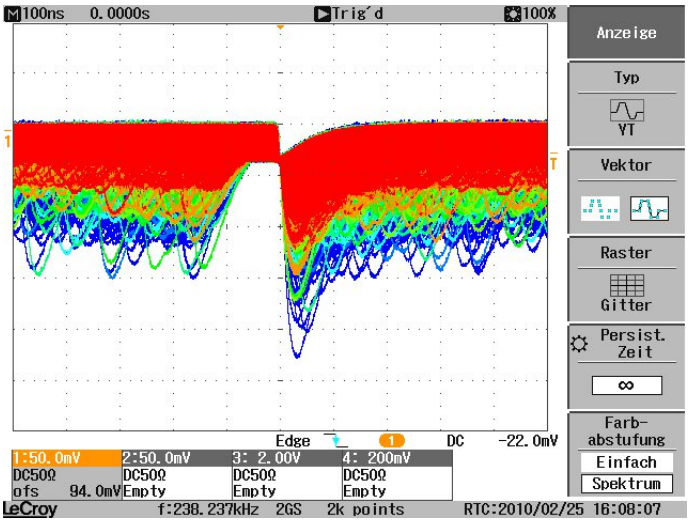

Figure 4.11.: *Noise of the SiPM*

4.5. Determination of the number of emitted photons per pulse

The picoamperemeter is able to measure the current in three different speeds of data taking, as mentioned in section 3.1.6. Obviously, the time over which the current is integrated is smaller if the speed is higher. Hence the slow mode[1] is chosen for all measurements in this experiment. To illustrate how important this decision is, histograms of the current distribution taken under same circumstances but with different speeds are shown in the figures 4.12(a) (fast)[2], 4.12(b) (medium)[3] and 4.13 (slow).

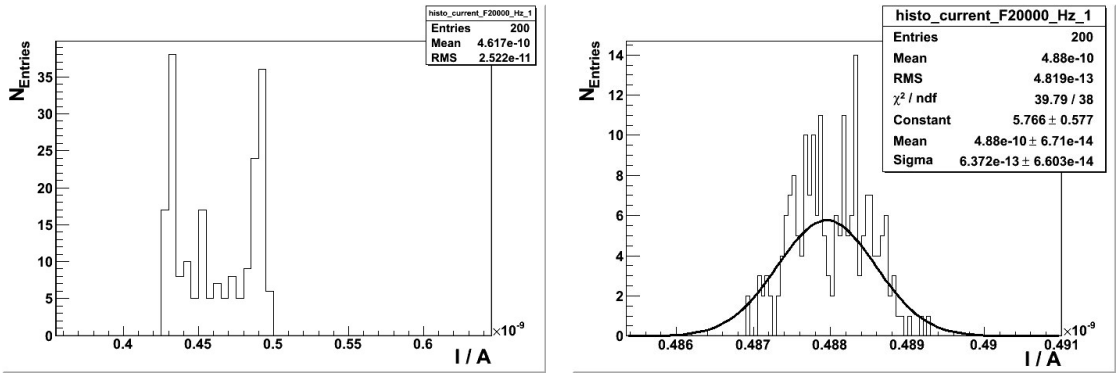

(a) Current distribution in fast mode at 20000 Hz pulse frequency and 3.0 V pulse height

(b) Current distribution in medium mode at 20000 Hz pulse frequency and 3.0 V pulse height

Figure 4.12.: *Current distribution of the picoamperemeter at different measurement speeds*

[1] measurement time corresponding to 5 power line cycles (PLC) of the supply voltage (230 V/50 Hz)
[2] measurement time corresponding to 0.1 PLC
[3] measurement time corresponding to 1PLC

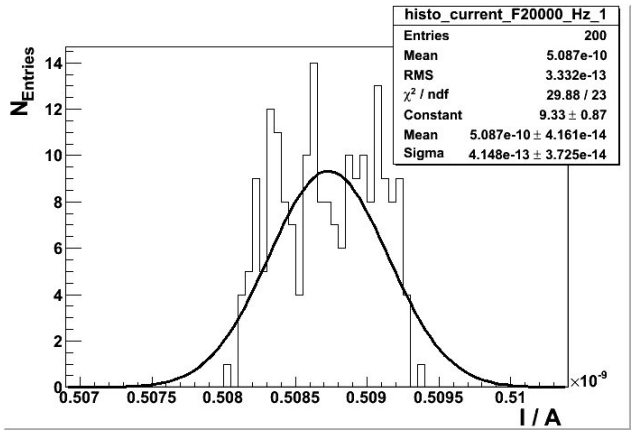

Figure 4.13.: *Current distribution in slow mode at* 20000 Hz *pulse frequency and* 3.0 V *pulse height. The black dots stand for fast, the blue squares for medium and the red triangles for slow mode.*

While the distributions in slow and medium mode have a gaussian character, in fast mode the current seems to jump between two major values, with values in between being much less likely. When comparing the means of the three different measurements, it can be seen that the three curves follow the same course. Figure 4.14 shows the behavior of the currents over the frequency,

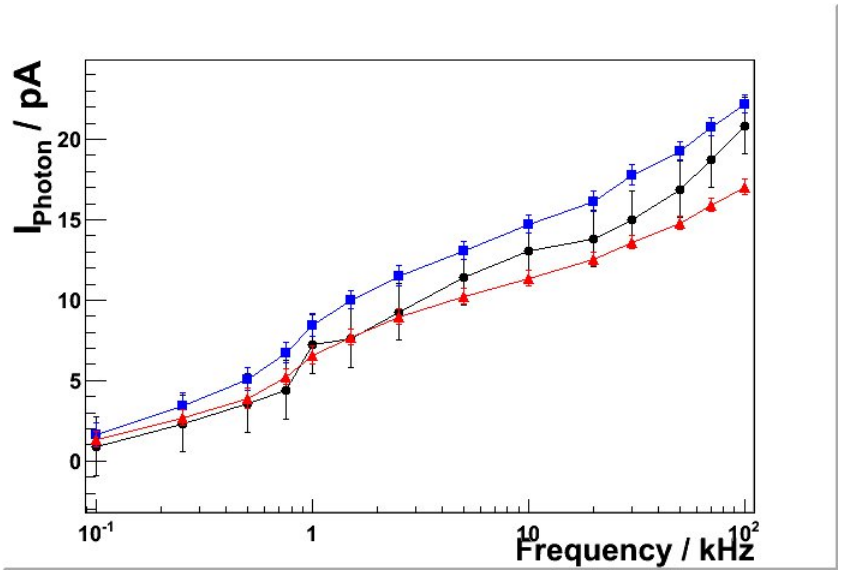

Figure 4.14.: *Currents over frequency at the three different speeds with logarithmic x-axis*

with a logarithmic x-axis for better visibility of the values at small frequencies. The values for fast mode are shown in black, the one for medium mode in blue and for slow mode in red.

The data taken during the measurement runs was processed with ROOT. There are two histograms for each of the 14 frequencies plus one for the baseline measured at the beginning of the measurement run. These were all read from the ROOT files and a the mean and its error were extracted. The mean of the baseline histogram is than subtracted from all the other one to get the current caused by the light of LED. By multiplying with the number of electrons in one Ampere ($6.24 \cdot 10^{18}$), the number of electrons per second that contributed to this currents is determined. As in a PIN diode each photon creates on pair of charge carriers, this corresponds to the number of

photons detected. To determine the real number of photons that reached the PIN diode, this value has to be divided by the quantum detection efficiency (QDE) at the wavelength of the photons. The photons emitted by the LED have a wavelength of about 400 nm. The quantum detection efficiency of the PIN diode at this point is 0.841, as can be seen in the calibration curve in the appendix B.

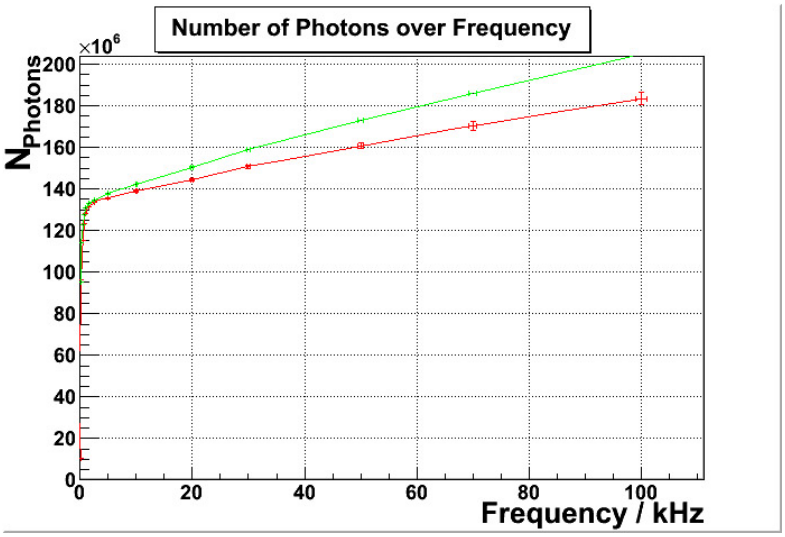

Figure 4.15.: *Number of photons over frequency at* 4.75 V *pulse height.*

Figure 4.15 shows the number of detected photons (corrected with the QDE and the baseline) over the frequency for the measurement made at 4.75 V pulse height. The red curve shows the measurements done before the QDC data taking at the frequency, the green one the measurements after the QDC data taking. Obviously the green curve lies above the red, which indicates that every time the measured current after the QDC data taking was slightly higher than the one measured before. This effect is visible throughout all measurements made is most likely caused by a systematic effect in the picoamperemeter, probably its reaction to temperature.

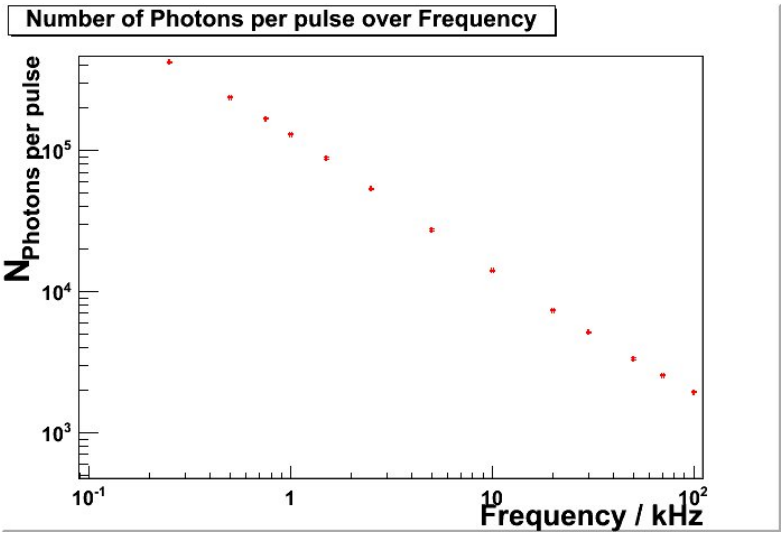

Figure 4.16.: *Number of photons per pulse over frequency at* 4.75 V *pulse height.*

Another interesting and unexpected effect is the general behavior of the number of photons. Ex-

pected was a linear relation between the frequency and the number of pulses, as the LED should emit the same number of photons per pulse at every frequency. As can be seen in figure 4.16 this is clearly not the case. It is assumed that the reason for this behavior can be found in the way that the picoamperemeter gets its current readings. The current is read into the internal buffer with a rate of 1000 Hz. After that, this values are averaged over as many power line cycles as selected. It is not known how long each of the 1000 readings per second is taken, but is seems likely that here is the place to search for the reason of the behavior of the number of photons as shown in figure 4.15. The two values of the photon number before and after the QDC measurement have been averaged and are shown over the frequency in a double-logarithmic scale. The number of photons per pulse drops rapidly with higher frequencies, resulting in the much less steep increase in the number of photons in this region as seen in figure 4.15. Figure 4.17 again illustrates the number of photons over the frequency. In this case the mean of the two graphs seen in 4.15 is shown. To the upper part of the frequency range, over 20 kHz, a linear fit could be made. The slope of the straight line gives the number of photons per pulse. As ca be seen, this is not a perfect estimation for the behavior of the photon number, but good as a first estimation. The region in which the fit was applicable is different for each pulse height Table 4.4 shows the results of the fits for the three

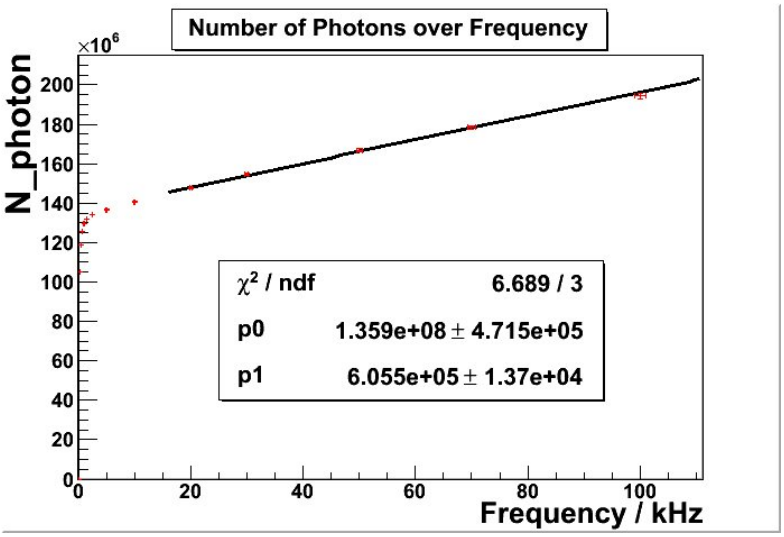

Figure 4.17.: *Number of photons over frequency at* 4.75 V *pulse height*

different pulse heights, the frequency region where they are applicable for and the baseline for the measurement. Surprisingly, the number of photons per pulse sinks with the pulse height. This

Pulse height[V]	Photons per pulse [$\cdot 10^5$]	Region of applicability [kHz]	Baseline [10^9 photons]
4.5	8.61± 0.11	30	4.577±0.001
4.75	1.36±0.14	20	5.158±0.010
5.0	1.02±0.03	20	5.291±0.008

Table 4.4.: *Number of photons per pulse for different pulse height*

effect is caused by the baseline, which is not stable and rises constantly over the day. As the three measurements were made on one day from morning until evening, the seen behavior of the photon number per pulse occurs. Suspected reason for this is the very high and unmonitored temperature in the laboratory.

4.6. Examination of SiPM response

The response of the SiPM to the light of the LED strongly depends on the number of photons that the LED emits. Figure 4.18 shows the response of the SiPM to a signal from the LED at a frequency of 10 kHz and a pulse height of 3.3 V. This measurement was done with the old LED-board without the termination resitor. The signal is displayed in yellow, the gate at the QDC in pink.

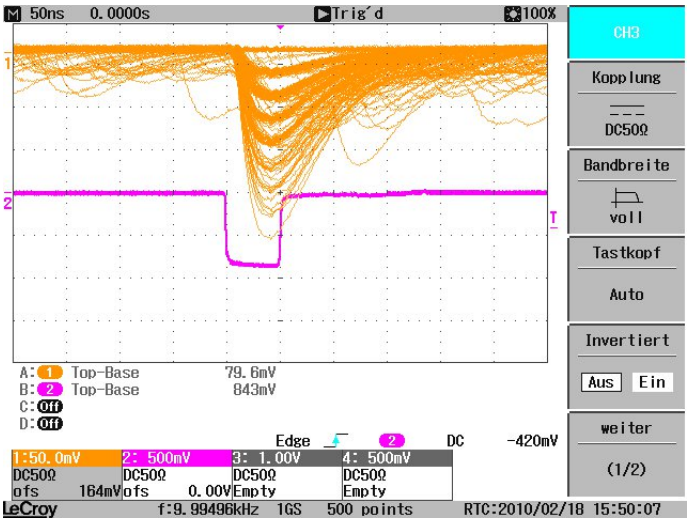

Figure 4.18.: *Signal of the SiPM at* 10 kHz *and an LED pulse height of* 3.3 V

Each thick line in the signal stands for one additional photon, the one closest to the baseline being the one photon peak, reaching up to eight photons in the highest pulse visible. As this is a snapshot of the signal, much more photons can be seen when the the display of the oscilloscope is set to spectrum with a persistance time of infinity. This is shown in figure 4.19. The highest pulse contributing to the spectrum seems to result from 12 photons hitting the SiPM at the same time.

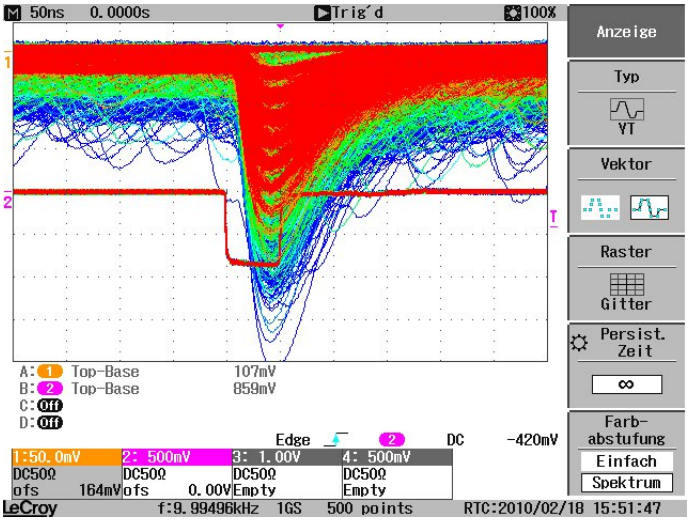

Figure 4.19.: *Signal of the SiPM with the same pulse properties as in figure 4.18, but with different display settings*

Important for the signal processing in the QDC is the gate width. The figures 4.18 and 4.19 show

the relation between signal and gate for a gate of 50 ns. The end of the gate lies shortly behind the peak of the signal. This improves the resolution of the SiPM spectra measured with the QDC as it is easier to distinguish between the amounts of charge corresponding to the respective number of photons when the tails are cut off.
If a gate of 75 ns is chosen, as is shown in figure 4.20, the situation changes. Now only a small part of the tails is cut off. The resolution worsens as the difference between the peaks becomes smaller. The advantage of this gate setting is, that only small parts of the tail are cut off. Therefore more of the charge generated in the avalanches inside the SiPM is collected by the QDC. The gain of the SiPM is therefore measured more correctly.

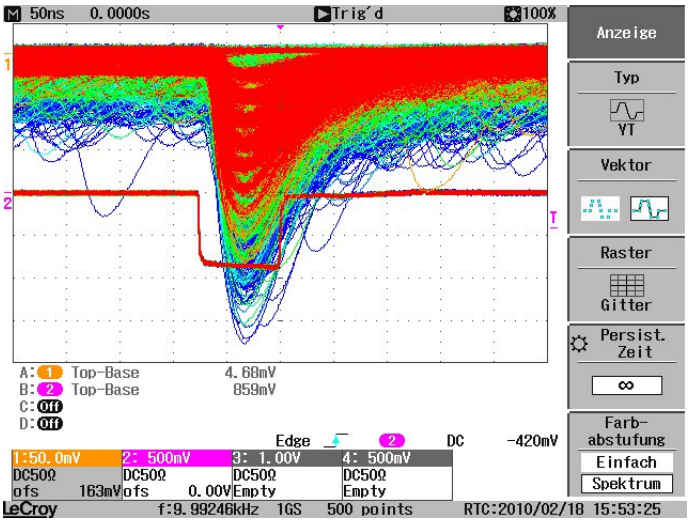

Figure 4.20.: *Signal of the SiPM with the same LED pulse properties as in figure 4.18, but with a* 75 ns *gate*

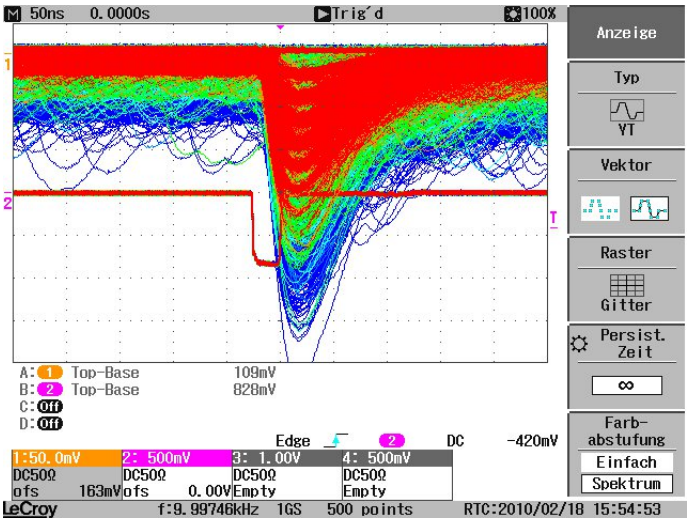

Figure 4.21.: *Signal of the SiPM with the same LED pulse properties as in figure 4.18, but with a* 25 ns *gate*

Figure 4.21 shows a very small gate of 25 ns. As can clearly be seen, the gate is to small to capture most of the signal. It can be seen in the SiPM spectra that this configuration leads to a too small

value of the gate and a bad resolution.
As an example, three SiPM spectra are shown in the figures 4.22(a), 4.22(b) and 4.22. All have been measured at a 100 ns gate and a frequency of 1000 Hz. To get a very good resolution, 1.5 million events were taken. They clearly show how the number of photons, that are emitted by the LED, can be adjusted by tuning the height of the pulses which drives the LED. It is obvious, that in this case a increase in the pulse height leeds to an increase in the number of photons emitted by the LED. This is another strong hint, that the strange results in section 4.5 are caused by a systematic effect in the current measurement. One effect discovered in the finishing stages of the

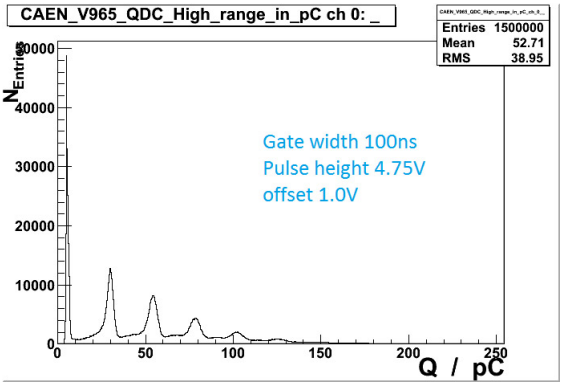

(a) SiPM spectrum at an LED pulse height of 4.5 V

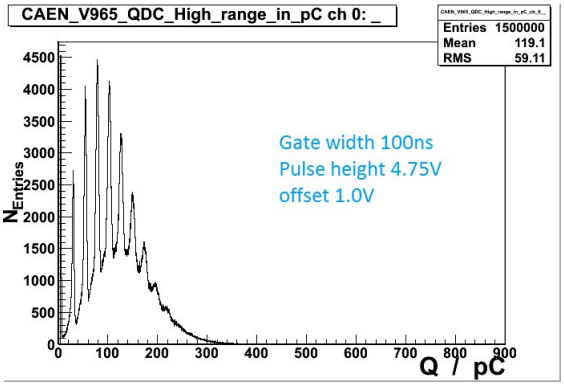

(b) SiPM spectrum at an LED pulse height of 4.75 V

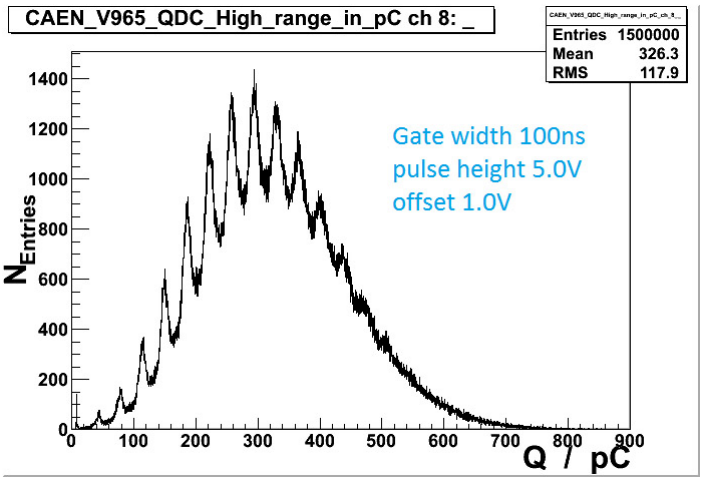

Figure 4.22.: *SiPM spectrum at a an LED pulse height of* 5.0 V

measurements is a resonance of the LED pulses in the SiPM signal. Figure 4.23 shows the impact of the LED pulse on the output of the amplifiers on the front-end electronics board. It can be seen that the resonance are in coincidence with the gate signal, a clear hint that it is caused by the pulses, which have the same frequency as the gate. This effect is caused by the small board used for the connection of the LED to the LEMO cable. As it was not shielded, it works as an antenna that sends out signals that influence the surrounding devices. After this behavior was discovered, a new board was built by the electronics workshop with additional shielding. This prevents the board from sending out signals. However, when the LED is plugged in to the new board, its legs also work as an antenna and cause resonances. They are smaller than they were before the shielding was applied. The resonances shown in figure 4.23 are the remaining effect after the new board with shielding was build. The impact of the effect on the SiPM signal can be

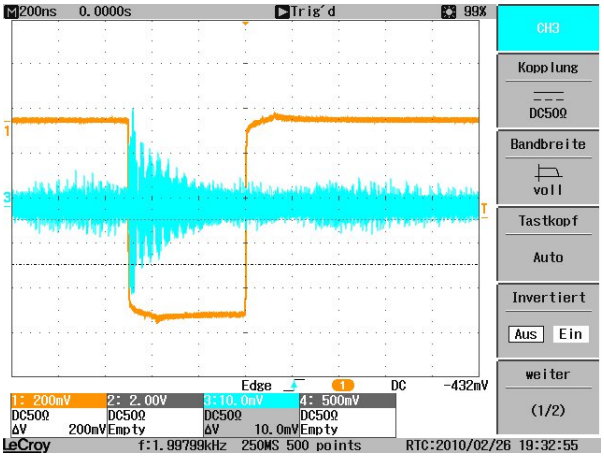

Figure 4.23.: *Resonance of the LED pulses in the output of the SiPM amplifiers*

seen in figure 4.24. This phenomenon was not discovered before because with the reflections of the signal at the LED, less of the signal was emitted and could interfere with the amplifier. Also the pulses were much smaller before the termination was implemented to the board. Fortunately the effect does not seem to prevent the QDC from taking good spectra, but for future measurements it will be necessary to shield the front-end electronics

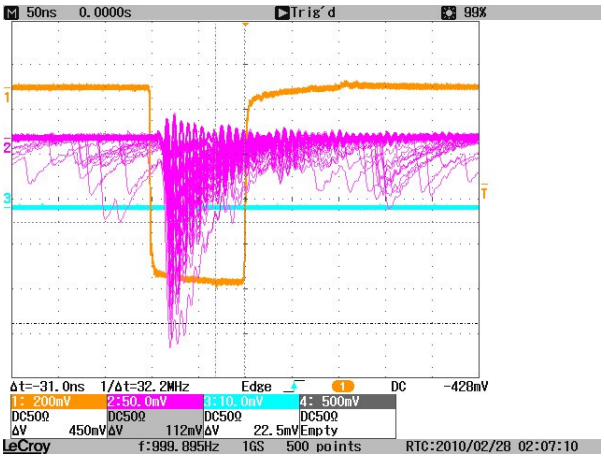

Figure 4.24.: *Resonance of the LED pulses in the output of the SiPM*

To take a more accurate look a their properties, SiPM spectra are shown for a frequency of 50 kHz with the y-axis set to a logarithmic scale. In all three diagrams the black line shows the spectrum for an LED pulse height of 3.3 V, the blue one shows the spectrum for 3 V pulse height and the red one for 2.7 V. Again, these are old measurements done without the termination resistor on the LED board. Figure 4.25 depicts the spectra for a gate width of 25 ns, figure 4.26 for a gate of 50 ns and figure 4.27 for a gate of 75 ns.

Apparently the influence of the gate widths as mentioned above can be seen in the diagrams. The spectra at a gate width of 25 ns are neither of a high resolution, nor do they allow for a good measurement of the gain, as the distance between two photo-electron peaks is strongly dependent of the LED pulse height. Therefore the configuration with a 25 ns gate is not useful and will not be considered in the future.

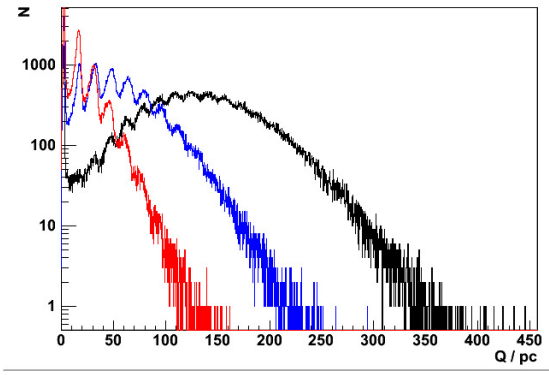

Figure 4.25.: *SiPM spectra at a gate width of* 25 ns

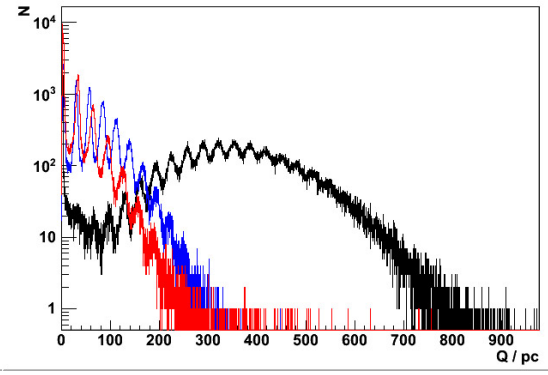

Figure 4.26.: *SiPM spectra at a gate width of* 50 ns

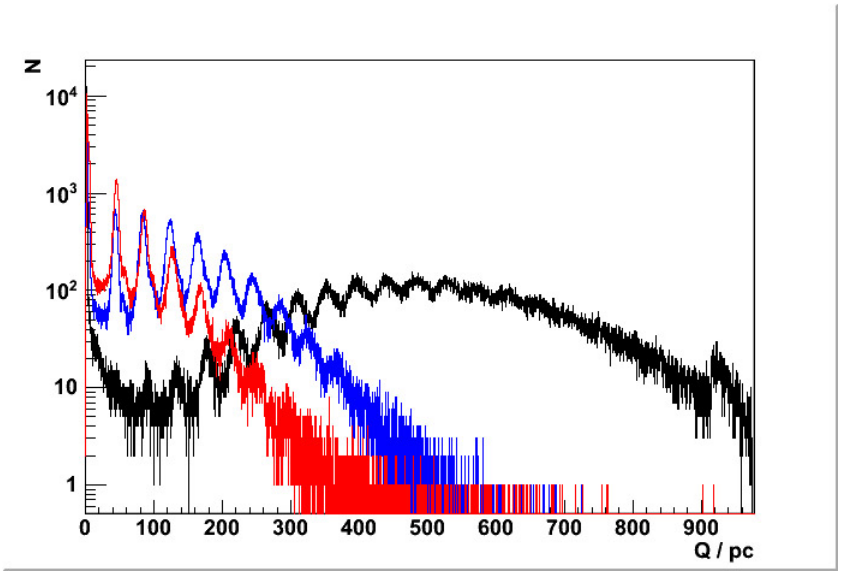

Figure 4.27.: *SiPM spectra at a gate width of* 75 ns

The 50 ns gate offers the best resolution, but here the distance between the the peaks is still hugely dependent on the pulse height of the LED. With the 75 ns gate, it is the other way around. The resolution becomes worse as more charge is admitted into the QDC during the gate time. This, on the other hand, lowers the dependency between peak distance and the pulse height. Also, if very many pixels are triggered during one gate time, the amount of charge admitted into the QDC becomes larger than the measurement range of the QDC, which can be seen at charges over 900 pC in figure 4.27.
The number of Photons visible in the three diagrams complies with the non-linear response of the LED to the forward voltage. Thus the step from 2.7 V to 3.0 V results in a much smaller increase of photon number than the step from 3.0 V to 3.3 V. For future measurements a gate of 100 ns is chosen because despite the loss of resolution, it seems not appropriate to cut away much of the signal. Figure 4.28 shows a noise spectrum measured with the setup. The y-axis is set to logarithmic scale Nearly no photon peaks are visible. This is due to the fact, that a random trigger of 1000 Hz is used. The SiPM has a noise frequency of about 650 kHz, the gate width is 100 ns in this case. This means, that $1000\,\text{Hz} \cdot 650\,\text{kHz} \cdot 100\,\text{ns} = 65\,/\text{s}$ events lie within the gate. For the 250000 events the measurement time was about 320 seconds, so only about 20000 events contained a SiPM signal. This is way the SiPM noise can not be seen because the histogram does not contain

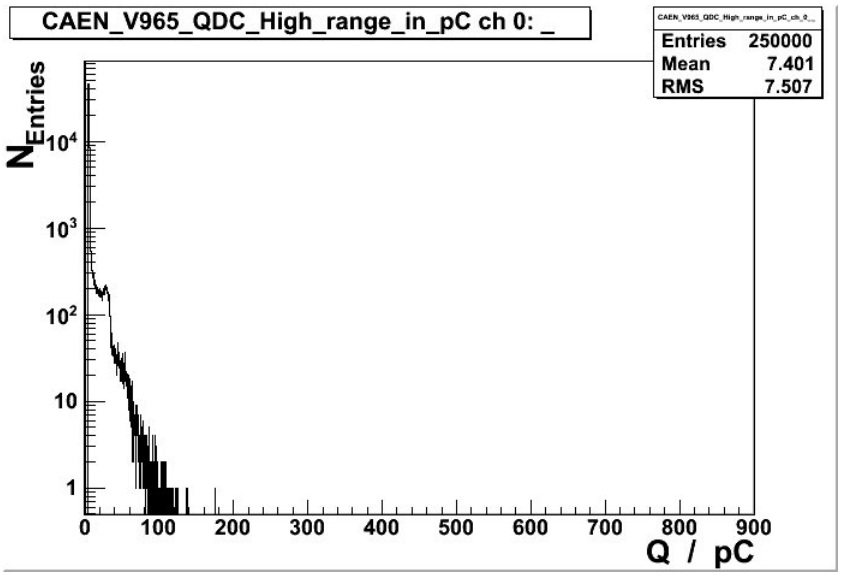

Figure 4.28.: *SiPM noise spectrum*

enough actual data.
The integrating sphere diffuses light with a high uniformity and there should be no differences between the different ports when it comes to the intensity of light. Nevertheless it is useful to confirm this be measuring with the SiPM mounted to two different ports. This was done at a pulse height of 3 V at a gate width of 75 ns. After the first run the positions of the PIN diode and the SiPM were switched. Due to the influence of the temperature described in 4.5, the current measurements taken in this runs are useless when it comes to comparing the quantity of the current measured, as the two runs were taken at different times of the day.
Nevertheless, the SiPM spectra can be compared and are shown in figure 4.29 It becomes clear,

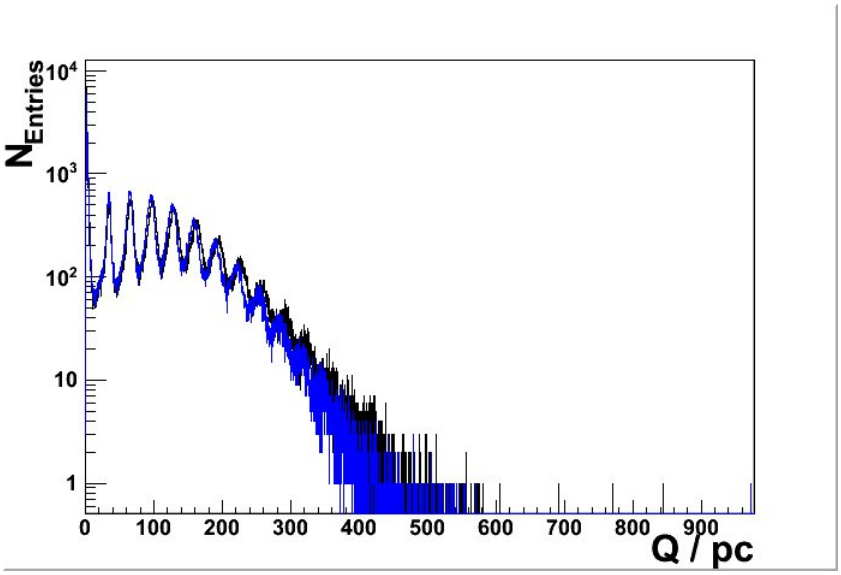

Figure 4.29.: *SiPM spectra measured at different ports of the integrating sphere*

that there is basically no difference between the ports, the integrating sphere works very well.

For the measurement of the quantum detection efficiency, the average number of photons seen by the SiPM has to be determined. This information can be gained from the SiPM spectra. As the number of photons is small, it is poisson distributed. The poisson distribution for variables x is given as:

$$f(x_1...x_n|\lambda) = \frac{e^{-\lambda} \cdot \lambda^{\sum_{i=1}^{n} x_i}}{x_1!...x_n!}. \tag{4.1}$$

Using the Maximum-Likelihood method an estimator for the expectation value λ of the distribution can be found. When a histogram of the measured data is given, where x_i stands for the detection of i photons and is found with the abundance h_i, the estimator $\hat{\lambda}$ can be calculated to

$$\hat{\lambda} = \frac{1}{\sum_{i=1}^{n} h_i} \sum_{i=1}^{n} x_i \cdot h_i. \tag{4.2}$$

Details on this can be found in appendix A.
As an exact determination of the number of photons is very elaborate, in this analysis only a very rough approximation is used. For this purpose the highest bin is taken from every photon peak and the pedestal. To compare the relative heights of the peaks, the number of entries of this highest bin is taken. As no consideration is made towards the shape of the peak, it is obvious how rough this method is. Using this data, the estimator of the poissonian distribution is calculated, along with the error on this value. Table 4.5 shows the estimated number of photon which are measured

Pulse Height[V]	Number of Photons
4.5	0.59 ±0.02
4.75	2.44±0.05
5.0	9.65±0.09

Table 4.5.: *Estimated number of photons seen by the SiPM at* 1 kHz *pulse frequency*

by the SiPM at a frequency of 1 kHz.
For one measurement at 4.5 V pulse height the average number of photons has been determined for all 14 frequencies. The behavior of the average photon number over frequencies is shown in figure 4.30. For the most part of the frequency range, the value is basically constant. This is the

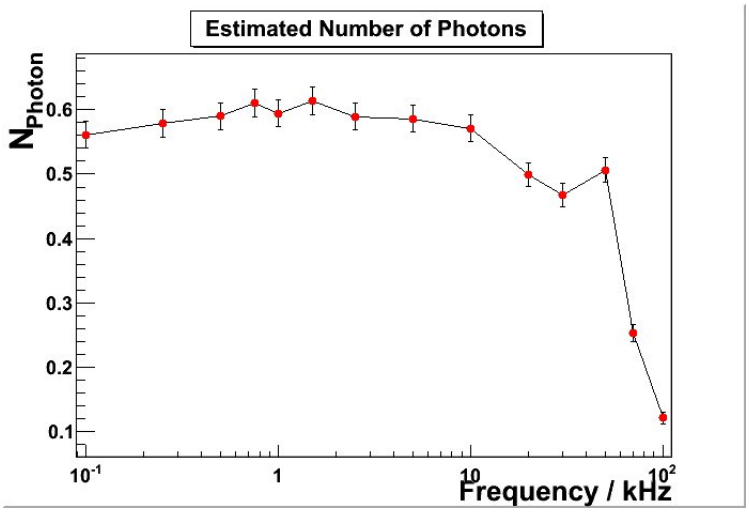

Figure 4.30.: *Behavior of the average photon number over frequency*

expected behavior, because the pulse frequency should have no influence on the number of photons

seen by the SiPM per pulse, if the distance between two pulses is larger than the recovery time of the SiPM. As the largest frequency used is 100 kHz, corresponding to a distance between the pulses of about 10 µs, this should not be a problem. Despite this, the average number of photon drops significantly after 20 kHz.

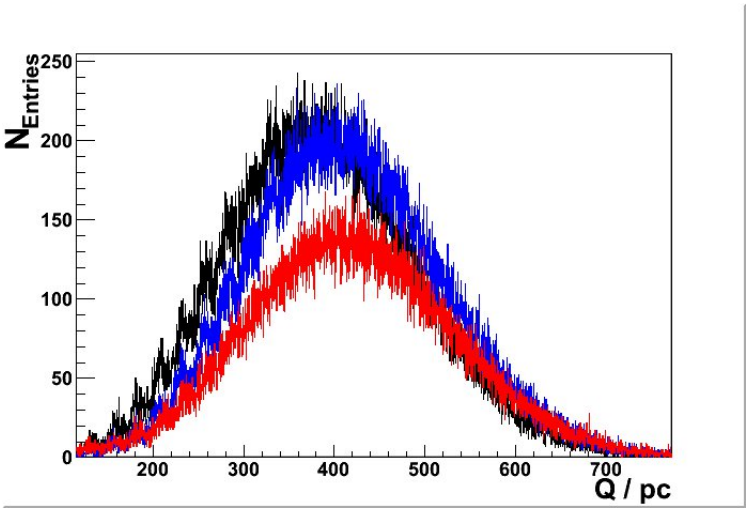

Figure 4.31.: *SiPM spectra at* 1 kHz, 20 kHz *and* 100 kHz

This behavior can be explained with the properties of the QDC. It turns out that the device cannot handle large readout frequencies. If the frequencies exceed 10 kHz, the QDC starts to measure an empty event unusually often. Therefore the pedestal rises while the heights of all the photon peaks shrinks. Therefore the result of the poisson estimation is shifted to smaller numbers. That the effect is very large can be seen in figure 4.31. It shows three spectra of a measurement with 5.0 V at three different frequencies. The black spectrum is for 1 kHz, the blue for 20 kHz and the red for 100 kHz. The x-axis is zoomed, so that the pedestal is not visible. Nevertheless the shrinking heights of the spectra can be seen. It has to be concluded that the QDC is not usable at this high frequencies, at least not with the latest software revision.

5. Outlook

In the past few months the development of a test stand for SiPMs has made good progress and many experiences on the properties of the different parts of the setup have been gained. Nevertheless, not all of the effects in the measurements are understood well enough and not all of the proposed features could yet be implemented.
Of the unclear systematic effects in the setup, the behavior of the LED is probably the one with the most impact on the overall measurements. It will certainly be investigated further, especially with regard to the influence of the newly implemented termination.
As the data taking with the QDC seems not to yield accurate results at the moment for higher frequencies, a lot of effort will be put into understanding the problems and finding solution for them. The first step will be to increase the readout performance of the QDC, which is possible with the newest versions of the respective liblab software. As this updates were released only days before its completion, it was not possible to implement the changes in time to include them into this thesis. Unfortunately, the behavior of the LED output and the readout limitations of the QDC lie on the opposite ends of the frequency range, making it hard to find a frequency region that suits both devices.
After the discovery of the resonances of the LED pulses in the SiPM signal, the shielding of the different components inside the dark box will be an important issue. The first step is made with the shielding of the LED, but this worked only to a certain extent.
Based on the results found in chapter 4.6, the gate width will be set to 100 ns in future measurements. This will render better measurements of the SiPM gain and ensure that basically all of the signal lies within the gate. The better resolution at lower gates is not important enough to accept the drawbacks. One major problem seems to be the temperature in the laboratory. As the current measurements with the picoamperemeter are extremely sensitive, they reflect the rising temperature over daytime. Unfortunately the laboratory in which the test stand is set at the moment does not offer any control over the temperature. Monitoring of the temperature will be one of the first improvements implemented in the near future
In the current state of the setup, the properties of the pulses have to be measured manually on the oscilloscope for each measurement. To automatize this, the readout of the oscilloscope via ethernet will be implemented into the measurement software. The driver for the readout has been finished, but due to limited time it was not possible to implement this feature into the software by now, as to date nobody has any experience using it.

One major drawback of the current setup is the limitation to one type of LED as a light source. This only allows for the measurement of the SiPM properties at at a certain wavelength. LEDs that emit light at different wavelengths would be the easiest solution for this limitation. To increase the precision of the measurements, a even better option would be to use laser diodes to have light with a far narrower wavelength distribution. The best solution however would be an adjustable light source that ca be tuned over a broad range of wavelengths. As building such a device is a huge project itself, it will be topic of another bachelor thesis in the next semester.

Concerning the analysis of the data taken in the experiment, the determination of SiPM properties from the QDC spectra was rather a rough estimation than a reliable analysis. This will hopefully be different in the future because of the implementation of a fit to the spectra. This fit is based on a procedure presented in [Bala]. It is based on the observation, that the SiPM spectrum is a convolution (R) of the pedestal (B) and the SiPM response to light (L). Using the fact, that the SiPM response the light is poissonian distributed and that the response of the SiPM to one photon is normal or log-normal distributed, it is possible to develop a fit procedure that can determine such important SiPM properties as the gain, crosstalk probability or the number of photons in a spectrum.

A. Maximum Likelihood Fit for Poisson Distribution

For the approximation of the average number of photons in an SiPM spectrum an estimator for the expectation value λ is needed. This is best provided by using the maximum likelihood fit.
This method is generally applicable for functions dependent on n values x_i and a parameter a. For this function $f(x_i, a)$ the likelihood $l(a) = \prod_i f(x_i, a)$ is defined. Using this, the following function can be defined [Hebbeker]:

$$L(a) = -2 \cdot ln(l(a)) = -2 \cdot \sum_i ln(f(x_i, a)). \tag{A.1}$$

To find the estimator for the parameter a the extremum of $L(a)$ has to be found.
In this case the function f is the poissonian distribution and the parameter a is the expectancy value λ:

$$f(x_i, \lambda) = \frac{e^{-\lambda} \cdot \lambda^{x_i}}{x_i!}. \tag{A.2}$$

Therefore the likelihood $l(\lambda)$ becomes:

$$l(\lambda) = \frac{e^{-n\lambda} \lambda^{\sum_{i=1}^{n} x_i}}{x_1!...x_n!}. \tag{A.3}$$

From this the function $L(\lambda)$ can be derived:

$$L(\lambda) = -2 \cdot ln(l(\lambda)) = -2(-2n\lambda) - 2ln(\lambda) \sum_{i=1}^{n} x_i + 2ln(\prod_{i=1}^{n} x_i!). \tag{A.4}$$

To find the estimator $\hat{\lambda}$, $L(\lambda)$ has to be differentiated and set to zero:

$$\frac{dL(\lambda)}{d\lambda} = \frac{2n - 2\sum_{i=1}^{n} x_i}{\lambda} \stackrel{!}{=} 0. \tag{A.5}$$

For the estimator this yields:

$$\hat{\lambda} = \frac{\sum_{i=1}^{n} x_i}{n}. \tag{A.6}$$

If the x_i are discrete values with an abundance h_i, the estimator becomes

$$\hat{\lambda} = \frac{\sum x_i \cdot h_i}{\sum h_i}. \tag{A.7}$$

B. PIN diode calibration

This figure shows the calibration curve of the PIN diode and the photon detection efficiencies at different wavelength as measured by Hamamatsu

HAMAMATSU
HAMAMATSU PHOTONICS K.K.

No. 1/1

FINAL INSPECTION SHEET

Date : Sep.18,2009

SPECTRAL RESPONSE CHARACTERISTIC

Type No. S9195 S/No. 1 Lot/No. 8G

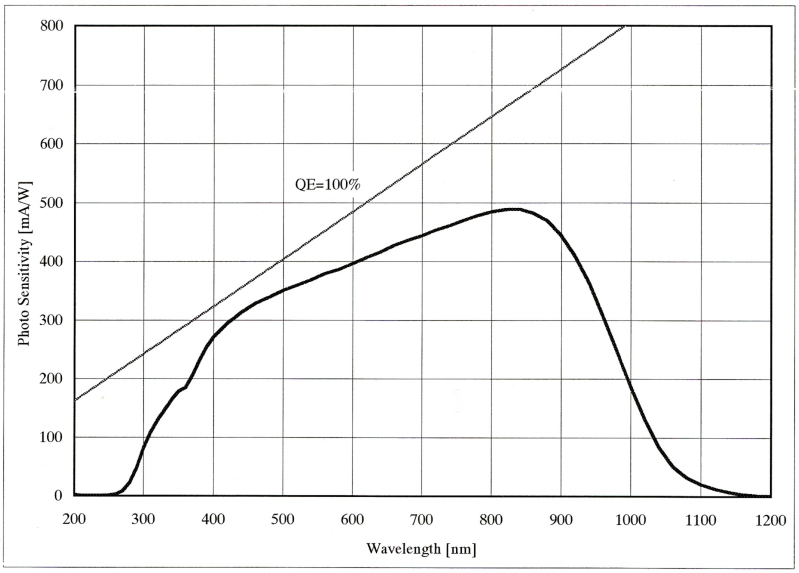

W.L. nm	S mA/W	Q.E. %	W.L. nm	S mA/W	Q.E. %	W.L. nm	S mA/W	Q.E. %	W.L. nm	S mA/W	Q.E. %
200	2	1.2	350	179	63.2	600	396	81.9	900	444	61.2
210	1	0.4	360	185	63.7	620	406	81.2	920	408	55.0
220	0	0.2	370	206	69.1	640	416	80.5	940	362	47.8
230	0	0.2	380	231	75.5	660	428	80.3	960	306	39.5
240	1	0.3	390	254	80.8	680	436	79.5	980	247	31.2
250	1	0.5	400	271	84.1	700	444	78.6	1000	187	23.2
260	3	1.2	420	295	87.0	720	453	78.1	1020	130	15.8
270	8	3.8	440	313	88.2	740	461	77.2	1040	84	10.0
280	22	9.8	460	329	88.6	760	470	76.6	1060	50	5.9
290	48	20.4	480	339	87.6	780	478	76.0	1080	32	3.6
300	81	33.3	500	351	87.0	800	484	75.1	1100	21	2.3
310	108	43.2	520	360	85.8	820	488	73.8	1120	13	1.4
320	129	49.9	540	369	84.6	840	489	72.2	1140	7	0.8
330	146	55.0	560	379	83.9	860	482	69.5	1160	3	0.3
340	163	59.5	580	386	82.6	880	469	66.1	1180	1	0.1

Date Inspected : Sep.18,2009 25°C

KAC-A028A

Figure B.1.: *Calibration curve and data for the PIN diode*

Bibliography

[Bala] V. Balagura, M. Danilov, B. Dolgoshein, S. Klemin, R. Mizuk, P. Pakhlov, E. Popva, V. Rusinov, E. Tarkovsky, I. Tikhominov - "Study of Scintillator Strip with Wavelength Shifting Fiber and Silicon Photomultiplier" - arXiv:physics/0504194v3 [physics.ins-det], http://arxiv.org/abs/physics/0504194v3

[BSSLab] Dr. S. Bosse BSS Lab Website http://www.bsslab.de/german/detekt.html, picture redone by M. Steinbrecher (University of Münster)

[Caen] Caen V965 QDC Manual, http://www.caen.it/getattach.php?mod=V965&obj=mn&id=2016

[Dol] B. Dolgoshein: "Silicon Photomultipliers in particle physics: possibilites and limitations", http://pc3k40.exp.mephi.ru/sipm/papers/sipm_final.pdf

[Günth 08/09] Prof. Güntherodt Experimentalphysik V, WS 08/09 Skript, RWTH Aachen

[Hama1] Hamamatsu S10362-11-100 Datasheet, http://sales.hamamatsu.com/assets/pdf/parts_S/s10362-11series_kapd1022e05.pdf

[Hama2] Hamamatsu S9195 PIN Diode Datasheet http://sales.hamamatsu.com/assets/pdf/parts_S/S9195.pdf

[Hebbeker] Prof. Thomas Hebbeker - Datenverarbeitung für Physiker WS06/07 Skript Kapitel 9, RWTH Aachen

[Herten] Prof. Gregor Herten - Experimentalphysik II, SS 2003, Uni Freiburg, hep.uni-freiburg.de/Lehre/ex2ss06/ueb/lha10.pdf

[Ibach09] Harald Ibach and Heinz Lüth: "Festkörperphysik Einführung in die Grundlagen" - Springer Verlag 2009

[Keithley] Keithley Picoamperemeter 6485 Manual, http://www.physics.fsu.edu/courses/Spring02/phy3802L/intlabdoc/instruments/keithley/6485_901_01A.pdf

[King] Kingbright UV-LED datasheet L-7113UVC, http://www.datasheetarchive.com/pdf-datasheets/Datasheets-16/DSA-308275.pdf

[Lecroy] Lecroy Wavejet 300 Series Datasheet, http://www.tequipment.net/pdf/LeCroy/WaveJet300Series_datasheet.pdf

[Lutz] Gerhard Lutz: "Semiconductor Radiation Detectors" - Springer Verlag 1999

[Mos] Moscow Engineering and Physics Institute, 'Pulsar' Enterprise, Lebedev Physical Institute - "An advanced study of silicon photomultipliers", http://www.slac.stanford.edu/pubs/icfa/fall01/paper3/paper3.pdf.

[Moser] Hans-Günther Moser: "Silicon Photomultipliers, A New Device For Low Light Level Photon Detection", http://edoc.mpg.de/353823

[Nutu] Norwegian Institute of Science and Technology - Website on solar cells, http://org.ntnu.no/solarcells/pages/pn-junction.php

[Pisa] University of Pisa - Functional Imaging and Instrumentation Group Website, http://www.df.unipi.it/~fiig/research_sipm.htm

[Plessen] Prof. G. von Plessen - Experimentalphysik III WS07/08 Skript - RWTH Aachen

[Renker] D. Renker: "Geiger-mode avalanche photodiodes, history, properties and problems", Nucl. Instr. Meth. A 567 (2008) 48-56

[Roper] "Entwicklung eines hochauflösenden Spurdetektors mit SiPM Auslese" - Gregorio Roper Yearwood, Diplomarbeit 2007, RWTH Aachen, I. Physikalisches Institut B

[SensL] SensL: "Introduction to the Silicon Photomultiplier", `http://www.sensl.com/pdfs/SPM_Tech_App_Notes/TN_Intro.pdf`.

[Thor] Thorlabs IS 200 Integrating Sphere datasheet, `http://www.thorlabs.de/Thorcat/13500/13574-S01.pdf`

[Wien] Wiener VM USB Manual, `www.wiener-d.com/Support/XXUSB/Manual_VM-USB_3_3.pdf`

[Wisc] University of Wisconsin - Madison Material Science and Research Center Website, `http://mrsec.wisc.edu/Edetc/background/LED/images/band_theory.JPG`, `http://mrsec.wisc.edu/Edetc/SlideShow/slides/pn_junction/pn_junction.jpg`

[Wiki] Wikipedia.org - Article on p-n junction, `http://en.wikipedia.org/wiki/File:Pn-junction-equilibrium-graphs.png`

List of Figures

Ich versichere hiermit, dass ich die Bachelorarbeit ohne fremde Hilfe und ohne Benutzung anderer als der angegebenen Quellen angefertigt habe. Alle Ausführungen der Arbeit, die wörtlich oder sinngemäß übernommen wurden, sind als solche gekennzeichnet.

Aachen, den 01.03.2010

(Jan-Frederik Schulte)

Acknowlegdements

I would like to thank Professor Thomas Hebbeker for the opportunity to write my thesis at his institute. I learned a lot in my time here, not only about my topic, but also about the LHC, CMS and data analysis. I would also like to thank him giving me the opportunity to continue my work on the test stand in the next semester and enabling me to visit the Introductory School on Terascale Physics at DESY in March.
Special thanks go to Dr. Markus Merschmeyer, who was a supervisor with great enthusiasm for the work down in the Tanzsaal, a constant source of inspiration and advice and had time for me even on weekends. I would like to thank Paul Papacz for teaching me a lot of the basics of Linux, C++ and ROOT and providing a lot of help and advice on many questions during the last months. Thank you to Carsten Mai for his advice on SiPM spectra.
Thanks to the CMS group of III. Physikalisches Institut A for a great work atmosphere and the many insights on data analysis and the CMS detector I got from their talks.
The electronics and mechanics workshop did great and fast work on all the parts they built for me in the last months, even in urgent situations. I am very grateful for their efforts.
Many many thank yous have to go to my family, who haven't seen much of me in the last months, but were extremely supportive of my work in all respects. Without them nothing of this would have been possible.
Thanks to all my friends, who provided much needed distraction from time to time and in the case of Manuel even a little help.